NASA Technical Paper 1868

April 1982

Fringe Localization Requirements for Three-Dimensional Flow Visualization of Shock Waves in Diffuse-Illumination, Double-Pulse Holographic Interferometry

Arthur J. Decker

NASA

NASA
Technical
Paper
1868

1982

Fringe Localization Requirements for Three-Dimensional Flow Visualization of Shock Waves in Diffuse-Illumination, Double-Pulse Holographic Interferometry

Arthur J. Decker
Lewis Research Center
Cleveland, Ohio

NASA
National Aeronautics
and Space Administration

**Scientific and Technical
Information Branch**

Trade names or manufacturers' names are used in this report for identification only. This usage does not constitute an official endorsement, either expressed or implied, by the National Aeronautics and Space Administration.

CONTENTS

Page

Summary 1

Introduction 1

Background 2

Rapid-Double Exposure Holography of a Shock Wave Experiencing Arbitrary Motion Between Exposures 5
- General Localization Condition 6
- Contributions to the Change in Refractive Index 7
- Representations of the Shock Wave 7
- Transformation of the Shock Wave 8
- The Difference in Refractive Index and its Gradient 8
- Localization Conditions for a Shock Wave 9
- Requirements for Localization 10
- Requirements for Accurate Localization 11

Rapid-Double-Exposure Holography of an Interblade Shock Wave in a Rotating Compressor 13
- Reference Frame Relative to a Particular Blade Passage 13
- Transformation of Coordinates at Second Exposure 14
- Representation $g(\mathbf{r}) = 0$ of the Shock Wave 14
- Treatment of Variation in Shock Strength $\Delta N(\mathbf{R})$ 14
- Expansion to First Order in α and Δn 15
- Localization Error Using a Polynominal Representation of the Shock Wave 17
- Final Comments on Localization Equations 34, or 35 and 36 18

Comparision of Localization Error Predictions with Holographic and Laser Anemometer Measurements in a Transonic Compressor Rotor 19
- Recording the Hologram 19
- Measurement of the Fringe Position in the Reconstructed Image 20
- Fringe Position at 100 Percent Speed Near Stall 21
- Measured Localization Error 23
- Calculated Localization Error 23
- Discussion of Results 24

Conclusions and Recommendations 26

Appendixes

A—Theory of Double-Exposure Holography for Diffuse Illumination of a Time Varying Phase Object 28

B—Effect of Wavelength Changes on Fringe Localization 35

C—List of Symbols 38

References 40

Summary

A theory of fringe localization in rapid-double-exposure, diffuse-illumination holographic interferometry is developed herein. A general theory of diffuse-illumination interferometry is the basis for a model to locate the interference fringes formed by arbitrary shock waves and, specifically, the shock waves in a rotating machine. The theory is then applied to the interpretation of holograms of the flow in a transonic axial-flow compressor rotor. The theory and laser anemometer measurements from the same compressor are used to compute the fringe localization error. The computed localization error is found to agree well with the measured localization error. Hence, the theory should serve as an adequate basis for designing measurement systems and experiments that use rapid-double-exposure holography.

In particular, it is shown how the curvature, positional variation in strength, and orientation of the shock wave relative to the viewing direction of the shock wave are all required to determine the localization error and to minimize it.

To accurately locate a shock wave, it is suggested that the view not deviate from tangency at the shock surface by more than 30°.

Introduction

Holography and laser anemometry have been used to study the flow in a rotating transonic compressor stage at the Lewis Research Center. Both methods are nonintrusive optical techniques specifically intended for use with flows in turbomachinery blade passages. Holography provides an instantaneous, entire field recording of the flow field while laser anemometry provides only a point measurement of the velocity. The objective is to provide detailed measurements within blade passages that are intended to verify new computational methods for compressor design and analysis (ref. 1).

As part of the program of holographic measurements to achieve this objective, over 200 double-exposure holograms of the flow between the blades of a transonic compressor rotor were recorded. The compressor operated between choke and stall at 75 to 100 percent of design speed. The method used for these measurements was rapid-double-exposure, diffuse-illumination, holographic interferometry. (See e.g., ref. 2).

Although the reconstructed holographic images contained the expected three-dimensional interference fringe pattern, it was obvious from the laster anemometer data that the fringes did not necessarily relate in a simple way to the shock waves creating them. In some cases the interference fringes coincided with the shock wave, but in others a fringe was substantially displaced from the shock wave. In the extreme, a fringe could not be associated with any finite location in space.

It was clear from the results that neither the models of double-exposure holography nor the analysis procedures for that technique were adequately developed. On the other hand, the simultaneous existence of holographic and anemometer data for comparison presented a unique opportunity to develop an accurate theory relating the shock and fringe locations.

In this paper, a theory of interference-fringe localization in rapid-double-exposure, diffuse illumination, holographic interferometry of moving shock waves is developed. The theory is compared with laser anemometer and holographic data from a transonic compressor rotor. Guidelines for the correct use of double-exposure holography are presented.

The main body of this report consists of three main sections. The first two develop the theory of fringe localization as it applies to rapid-double-exposure holography of shock waves. The third section compares the results of that theory with holographic and laser anemometer measurements from a rotating transonic compressor rotor. In the main body of the report, the principles of diffuse illumination interferometry are applied only to shock waves, and the case of a shock wave in a compressor rotor is emphasized.

The details necessary to develop the theory and to compare the theory with the measurements are left to the appendices. A general theory of diffuse illumination holographic interferometry is presented in appendix A. This theory makes liberal use of the presentation in Vest's book, Holographic Interferometry (ref. 3), with emphasis on those aspects of the theory that apply to shock-wave visualization. It is recommended that a reader not familiar with the theory of diffuse illumination interferometry read this appendix first, since some essential assumptions are discussed therein.

Because the wavelengths of the lasers used to record the hologram and to reconstruct the scene may be different, the effect of a wavelength change in reconstruction is discussed in appendix B.

Before developing the theory, the background of double-exposure holography is next summarized in more detail.

Background

Rapid-double-pulse, or rapid-double-exposure, holography was certainly appropriately named by Heflinger and Wuerker (ref. 2). The name refers to a doubly exposed hologram recorded with a very short time between exposures. The method is used for three-dimensional flow visualization of shock waves. The idea is straightforward and simple when applied to recording holograms in rotating compressor and fan stages.

As shown schematically in figure 1, diffused light from a pulsed laser is transmitted through a large window located upstream of a compressor stage. The light passes between the blades of the compressor and exits through a small window located over the blade tips. The light then falls on a high-resolution photographic plate, or film, which is also exposed to a reference beam. The hologram is recorded while the machine is rotating. (See ref. 4 for a general discussion of holography.) After the compressor has rotated through a small angle (of

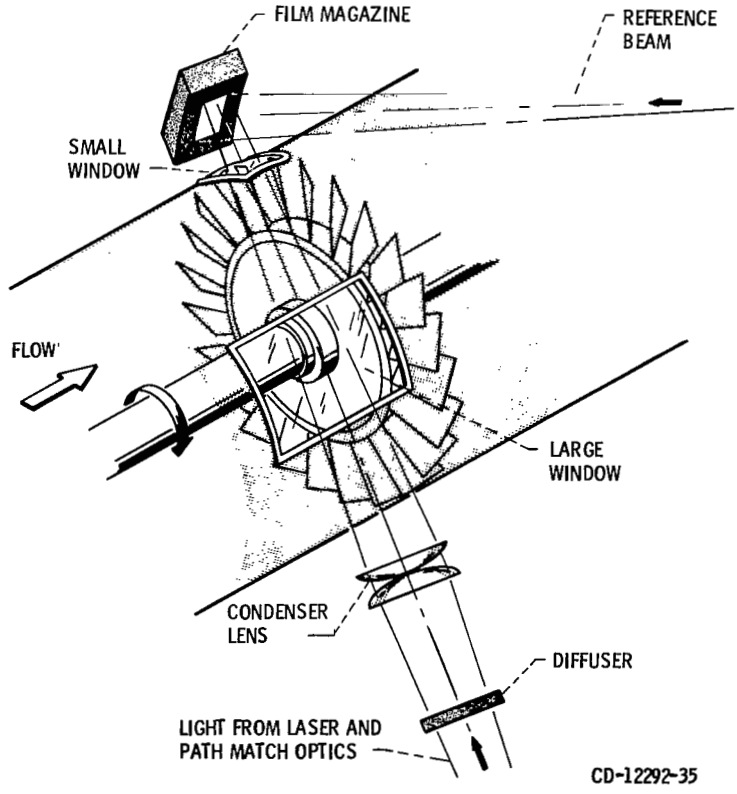

Figure 1. - Holography in single-stage compressor test facility.

the order of 0.01 rad.), a second hologram is recorded on the same film. When the double image is reconstructed, interference fringes are formed because of the slight difference in the refractive index fields between the two exposures. Provided that the windows and other optical components have not moved between the two exposures, the fringes are due entirely to the slight shift in the interblade flow field.

Instructions for building a system to record rapid-double-pulse holograms in rotating machines appear in other publications, and can be summarized quite briefly. First, the object is illuminated and the hologram is recorded in a so-called holocamera configuration (refs. 2 and 5) that compensates for the possible lower coherence property of pulsed solid-state lasers (ref. 6). Simply put, the holocamera, such as the one shown schematically in figure 2, is a form of interferometer. Reference-beam and object-beam rays from the same point on the holocamera beam splitter are routed through their respective optical trains so that they are brought back together at the same point on the hologram film. Care is taken to ensure that an object-beam–reference-beam ray pair travels about the same optical distance before intersecting at the film. (Optical distance is defined to be $\int nds$ where s is the geometrical path length of a light ray and n is the refractive index along the ray trace.)

In the compressor application, the object beam polarization is tailored to avoid showing fringes induced by stresses in the windows. One approach is to select a diffuser that completely depolarizes the object beam (ref. 7). In addition, a timing system must be constructed to fire the laser at the instant the blade passage of interest appears in a chosen location. One example of a timing system is the general purpose electronic shaft angle encoder for rotating machines described in reference 8.

The laser must produce pulse pairs for the double exposure. Most commerically available pused-ruby and neodynium YAG lasers are sold with this feature as well as with synchronization inputs to be used with an external clock.

Since test-section windows do not, in principle, move between exposures, they do not produce fringes, and their quality merely affects the quality of the hologram image. The setup described in reference 2 uses molded windows. At Lewis in the single-stage compressor test facility, the large window (depicted in fig. 1) is machined from plexiglass. The small window over the blade tips is machined from polysulfone a material that can withstand the higher temperature over the blades. Television quality resolution is obtained through the small window.

As a final step, a plate magazine or film transport may be required if a number of holograms are to be recorded without access to the test area. A glass-plate magazine is described in reference 2. At Lewis a 105-millimeter film transport is used to hold and to advance the holographic film.

Although each application of rapid-double exposure holography will require a different setup, the essential features of most systems have been outlined above. In figures 3(a) and (b) two photographs of the holography setup used in the single-stage compressor rig at Lewis are shown. The design of that holography system was based on the information of reference 2.

When a rapid-double-exposure hologram of a compressor flow containing shock waves is recorded, the interference fringes have a remarkable property. They appear to be located on, or

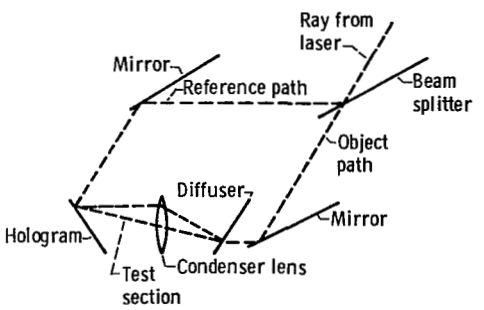

Figure 2. - Diagram of object and reference-ray path matching in holocamera configuration.

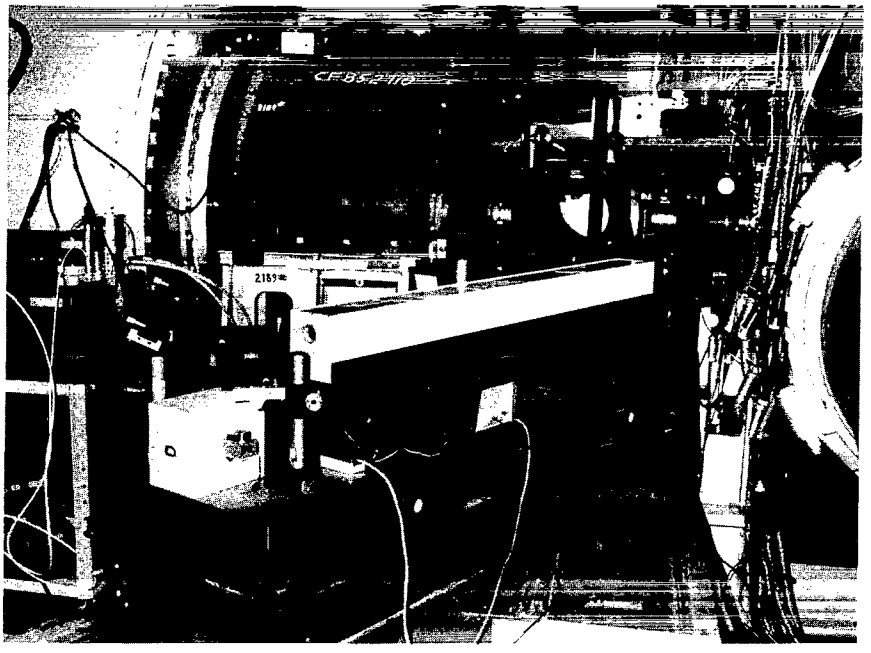

(a) Holocamera assembly.

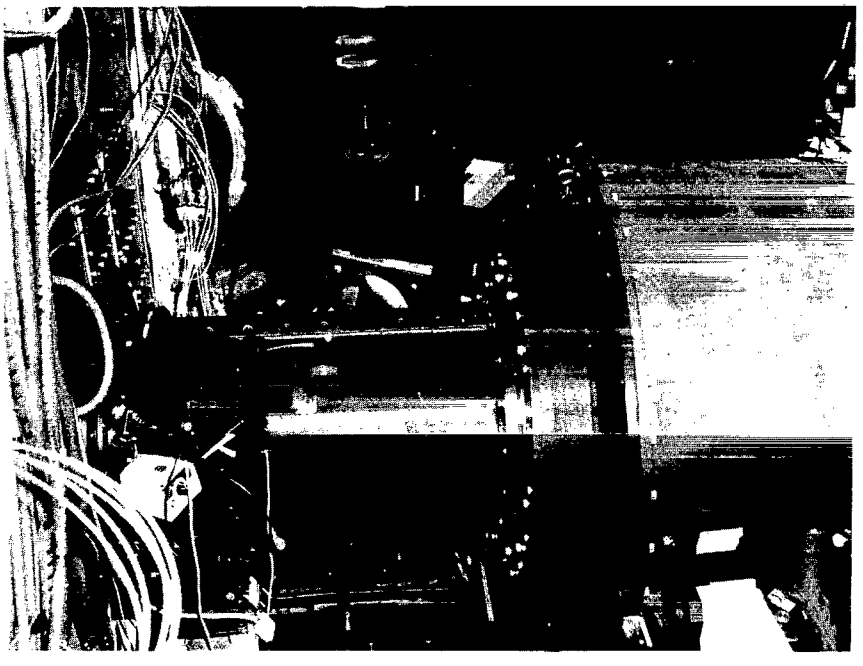

(b) From background to foreground, holocamera assembly, small window, and film magazine.

Figure 3. - Experimental setup.

localized on, surfaces. These surfaces look like shock waves. A photograph of such a fringe pattern for a Lewis compressor near stall is shown in figure 4. Indeed, it is easy while viewing the reconstructed image to make a pencil tip coincide with the fringe location. From a particular viewing direction, the surface can be traced either by measuring its location photogrammetrically with an XYZ translation stage and a self-illuminated pointer or by tracing the apparent fringe boundaries with glue filaments (ref. 2).

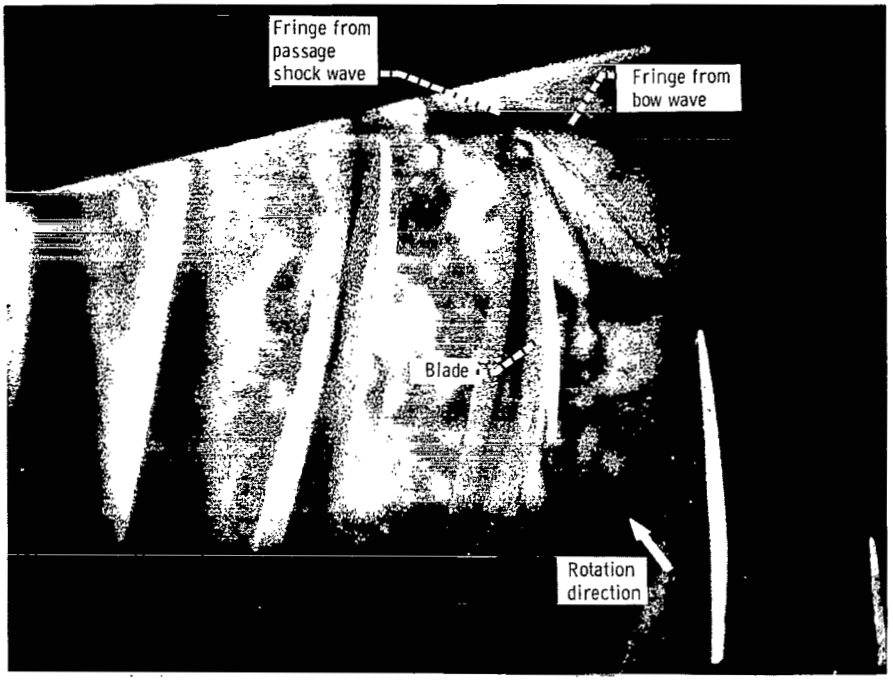

Figure 4. - Interference fringe due to bow and passage shock waves in a transonic compressor rotor.

Unfortunately, in spite of its suggestive appearance, a fringe does not necessarily coincide with the shock wave that created it. In fact, if a plane shock wave having uniform strength is moved arbitrarily between exposures and the reconstructed image is viewed from an arbitrary vantage point, the fringe can appear to be localized anywhere between a true position of the shock wave and infinity.

Clearly, the difference between the fringe and shock location, which will be called fringe-localization error, compromises the usefulness of rapid-double-exposure holographic interferometry. For example, in choosing a vantage point for recording a hologram of a shock wave, one is usually severely constrained by the geometry of the equipment used to generate the shock wave. We show later in this report that a relatively steep view (one that approaches tangency to the shock wave surface) minimizes the localization error. A fan with a large ratio of blade-tip radius to hub radius such as the fan reported in reference 2 allows a more tangent view than a compressor with a small radius ratio such as the one operated in the Lewis single-stage compressor test facility. If a steep view is not possible, then a designer of a rapid-double-exposure holography system for a compressor may decide that the technique is not useful.

However, for unsteady flows the instantaneous recording capability of holography is irreplaceable. At the same time there are flow situations such as through cascades and fans having large span where a selection of views is available.

To caution against the indiscriminant use of rapid-double-exposure holography and to provide design assistance where double-exposure holography is the only alternative or where a broad selection of views is available, a theory of fringe localization is developed. The theory is compared with laser anemometer and holographic data recorded in the single-stage compressor rig at Lewis.

Rapid-Double-Exposure Holography of a Shock Wave Experiencing Arbitrary Motion Between Exposures

In this section, the theory of rapid-double-exposure holography developed in appendix A is applied to a generally curved shock wave whose strength depends on position. The conditions

for good fringe localization (sharply defined fringes) and accurate localization (fringes located near one of the two positions of the shock wave) are determined.

General Localization Condition

If the *change* in refractive index is given by the function $f(\mathbf{r})$ where $\mathbf{r} \equiv (x,y,z)$ (see fig. 5) and if the reconstructed image is viewed from a *fixed* direction defined by the unit vector $\mathbf{k}$ directed to the center of the viewing aperture, then the interference finge(s) appears to be located at positions $\mathbf{r_f} \equiv (X, Y, \mathcal{Z})$ determined by equations (1) from appendix A. Note that all symbols are also defined in Appendix C. The localization equations as derived in appendix A are

$$\mathcal{Z} = \frac{\int_{-\infty}^{\infty} \nabla f \cdot \mathbf{K}_x z dz}{\int_{-\infty}^{\infty} \hat{\imath} \cdot \nabla f dz} \qquad \mathcal{Z} = \frac{\int_{-\infty}^{\infty} \nabla f \cdot \mathbf{K}_y z dz}{\int_{-\infty}^{\infty} \hat{\jmath} \cdot \nabla f \, dz} \tag{1}$$

where the substitution

$$\mathbf{r} = \mathbf{r}_f + \mathbf{k}\frac{(z - \mathcal{Z})}{k_z}$$

is made before integration. The vectors $\mathbf{K}_x$ and $\mathbf{K}_y$ are defined by the equations

$$\mathbf{K}_x = [k_y^2 + k_z^2, -k_x k_y, -k_x k_z]$$

$$\mathbf{K}_y = [-k_x k_y, k_x^2 + k_z^2, -k_y k_z]$$

The vector $\mathbf{K}_x$ is perpendicular to the viewing direction and is in the plane containing the viewing vector $\mathbf{k}$ and the x axis. The vector $\mathbf{K}_y$ is perpendicular to the viewing direction and is in the plane containing the viewing vector $\mathbf{k}$ and the y axis.

The limits of the integrals in equations (1) are $(-\infty,\infty)$ subject to the assumption and realization that $f(\mathbf{r})$ will be nonzero in a limited region. Each of the two equations (1) defines a surface where $\mathcal{Z}$ can be expressed as a function of X and Y. The two equations together generally define a curved line. Hence, the fringes localize in the neighborhood of that line. The actual region where the fringes have high visibility is determined by the modified depth-of-field described in appendix A.

One of the two equations (1) may be satisfied only in the trivial sense; that is, one of the

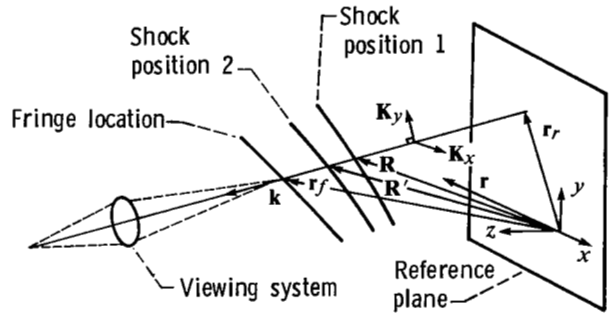

Figure 5. - Reference plane and vectors used to apply fringe localization theory to interpret interference fringes associated with shock waves in compressor rotor.

two localization equations may be satisfied for all positions $\mathbf{r}_f$. This condition will occur if the change in phase

$$\Delta\theta = \frac{2\pi}{\lambda}\int_{-\infty}^{\infty} f(\mathbf{r})\frac{dz}{k_z}$$

along a ray passing through the arbitrary point $\mathbf{r}_f$ and the point

$$\mathbf{r}_r \equiv (x,y,0)$$

on the reference plane (fig. 5) depends not at all or only weakly on x or y. If $\Delta\theta$ depends weakly on x, then the first of equations (1) is satisfied for all $\mathbf{r}_f$. The expression *weak dependence* rather than *no dependence* is emphasized since the nonzero depth of field of the viewing system will prevent a slowly varying derivative of $\Delta\theta$ from establishing localization. This conclusion can be drawn by examining equation (A13) in appendix A.

In fact, for visualizing a shock wave, it is desirable that only one of the two equations (1) apply. Then localization will occur on a surface. In some cases, this surface can coincide with the shock wave.

Contributions to the Change in Refractive Index

It will be assumed that a view can be found where the shock wave of interest dominates the integrals. There is a possibility that can invalidate this assumption. This possibility consists of a flow features that contribute smaller values of ∇f than the shock wave, but contribute over larger distances.

Representation of the Shock Wave

Because a shock wave is very thin, the change in refractive index across the shock can be represented very nearly by a step function. The location of this step is a generally curved surface given by an equation having the general form

$$g(\mathbf{r}) = 0 \tag{2}$$

There are several functions that pass to the step function in the limit of decreasing width (ref. 9). The refractive-index function N that will be used to represent a shock wave is given by the equation

$$N = N_0 + \frac{\Delta N}{\pi}\tan^{-1}[ag(\mathbf{r})] \tag{3}$$

In equation (3), the number a is made arbitrarily large. Then, when $g(\mathbf{r})<0$, N approaches $N_0 - (\Delta N/2)$ in a very short distance. When $g(\mathbf{r})>0$, N approaches $N_0 + (\Delta N/2)$ in very short distance. When $g(\mathbf{r})=0$, $N=N_0$.

Not only does $g(\mathbf{r})$ have an arbitrary shape, both N_0 and ΔN may be functions of position. However, the contribution of N_0 to any derivatives of N will be negligible when compared with the contribution of

$$\frac{\Delta N}{\pi}\tan^{-1}[ag(\mathbf{r})]$$

The value of ΔN will be called the shock strength.

The mathematical representation of the motion of the shock wave between the two exposures is derived next.

Transformation of the Shock Wave

Between exposures, a shock wave can be rigidly translated, rotated, or deformed. In this paper, only translation and rotation are considered. The case of rigid translation and rotation applies to steady flows in rotating machines. The shape of the shock wave might change in unsteady flows.

In the steady-flow case considered in this report, the shock wave is pictured as being rigidly attached to a coordinate system. At the first exposure the coordinate system is chosen to be the reference frame. Between the first exposure and the second exposure, the coordinate system undergoes a rigid translation and rotation. The shock wave has the same equation in the transformed coordinates at the second exposure as it has in the reference frame at the first exposure. That is,

$$g(\mathbf{r}) = 0$$

$$g(\mathbf{r}_t) = 0$$

where $\mathbf{r} \equiv (x,y,z)$ represents the coordinates in the reference frame and $\mathbf{r}_t \equiv (x_t,y_t,z_t)$ represents the coordinates in the transformed system. Hence, to obtain the equation of the shock wave at the second exposure, the vector $\mathbf{r}_t$ in $g(\mathbf{r}_t) = 0$ is simply transformed in terms of $\mathbf{r}$. The transformation of coordinates is given by the expression

$$\mathbf{r}_t = \bar{\Gamma} \cdot \mathbf{r} + \mathbf{d} \tag{4}$$

where dyadic notation is used.

In equation (4) the matrix $\bar{\Gamma}$ is the 3 by 3 matrix of the direction cosines of the axes of the transformed system measured relative to the axes of the reference frame, that is,

$$\bar{\Gamma} = \begin{pmatrix} \cos\alpha_x & \cos\alpha_y & \cos\alpha_z \\ \cos\beta_x & \cos\beta_y & \cos\beta_z \\ \cos\gamma_x & \cos\gamma_y & \cos\gamma_z \end{pmatrix}$$

The vector $\mathbf{d} \equiv (d_x,d_y,d_z)$ defines the translation.

The Difference in Refractive Index and its Gradient

From equation (3), the difference in refractive index $f(\mathbf{r})$ between the first and second exposures is given by the equation

$$f(\mathbf{r}) = N_0(\mathbf{r}_t) - N_0(\mathbf{r}) + \frac{\Delta N(\mathbf{r}_t)}{\pi} \tan^{-1}[ag(\mathbf{r}_t)] - \frac{\Delta N(\mathbf{r})}{\pi} \tan^{-1}[ag(\mathbf{r})] \tag{5}$$

where $\mathbf{r}_t$ is determined from equation (4).

In equation (5) both N_0 and ΔN are functions of position. However, the derivatives of N_0 and ΔN are small in comparison with the derivatives of $\tan^{-1}[ag]$ and are ignored. Differentiating equation (5) subject to this assumption and applying equation (4), the gradient ∇f is given by

$$\nabla f(\mathbf{r}) = \frac{\Delta N(\mathbf{r}_t)}{\pi} \frac{a}{1+a^2g^2(\mathbf{r}_t)} \nabla_t g(\mathbf{r}_t) \cdot \bar{\Gamma} - \frac{\Delta N(\mathbf{r})}{\pi} \frac{a}{1+a^2g^2(\mathbf{r})} \nabla g(\mathbf{r}) \tag{6}$$

where ∇_t implies differentiation with respect to the coordinates in the transformed system.

At this stage, it is convenient to note that $a/(1+a^2g^2(\mathbf{r}))$ is a very narrow function of $g(\mathbf{r})$. It is convenient and correct to replace it with the Dirac delta function:

$$\lim_{a\to\infty}\frac{a}{1+a^2g^2(\mathbf{r})}=\pi\delta[g(\mathbf{r})]$$

$$\lim_{a\to\infty}\frac{a}{1+a^2g^2(\mathbf{r}_t)}=\pi\delta[g(\mathbf{r}_t)]$$

Equation (6) becomes

$$\nabla f(\mathbf{r})=\Delta N(\mathbf{r}_t)\nabla_t g(\mathbf{r}_t)\cdot\bar{\Gamma}\,\delta[g(\mathbf{r}_t)]-\Delta N(\mathbf{r})\nabla g(\mathbf{r})\,\delta[g(\mathbf{r})] \tag{7}$$

Localization Conditions for a Shock Wave

The procedure for determining the localization conditions for the shock wave is easily stated: Equation (4) is substituted into equation (7); the relationship $\mathbf{r}=\mathbf{r}_f+\mathbf{k}(Z-\mathcal{Z})/k_z$ is substituted into equations (1); the integrals in equations (1) are then evaluated. Substituting equation (7) into equations (1), the integrals in equations (1) assume the form

$$\mathcal{Z}=\left\{\int_{-\infty}^{\infty}\Delta N(\mathbf{r}_t)\nabla_t g(\mathbf{r}_t)\cdot\bar{\Gamma}\cdot\mathbf{K}_x\delta[g(\mathbf{r}_t)]z\,dz-\int_{-\infty}^{\infty}\Delta N(\mathbf{r})\nabla g(\mathbf{r})\cdot\mathbf{K}_x\delta[g(\mathbf{r})]z\,dz\right\}\Bigg/$$

$$\left\{\int_{-\infty}^{\infty}\Delta N(\mathbf{r}_t)\hat{\imath}\cdot\nabla_t g(\mathbf{r}_t)\cdot\bar{\Gamma}\delta[g(\mathbf{r}_t)]dz-\int_{-\infty}^{\infty}\Delta N(\mathbf{r})\hat{\imath}\cdot\nabla g(\mathbf{r})\delta[g(\mathbf{r})]dz\right\}$$

$$=\left\{\int_{-\infty}^{\infty}\Delta N(\mathbf{r}_t)\nabla_t g(\mathbf{r}_t)\cdot\bar{\Gamma}\cdot\mathbf{K}_y\delta[g(\mathbf{r}_t)]z\,dz-\int_{-\infty}^{\infty}\Delta N(\mathbf{r})\nabla g(\mathbf{r})\cdot\mathbf{K}_y\delta[g(\mathbf{r})]z\,dz\right\}\Bigg/$$

$$\left\{\int_{-\infty}^{\infty}\Delta N(\mathbf{r}_t)\hat{\jmath}\cdot\nabla_t g(\mathbf{r}_t)\cdot\bar{\Gamma}\delta[g(\mathbf{r}_t)]-\int_{-\infty}^{\infty}\Delta N(\mathbf{r})\hat{\jmath}\cdot\nabla g(\mathbf{r})\delta[g(\mathbf{r})]dz\right\} \tag{8}$$

Some additional variables are defined and explained at this point. Let $\mathbf{R}$ be that value of $\mathbf{r}$ where the viewing axis intersects the first position of the shock wave. Then $g(\mathbf{R})=0$. Let Z be the corresponding value of z.

Let $\mathbf{R}'$ be the value of $\mathbf{r}$ where the viewing axis intersects the second position of the shock wave. Let Z_t be the corresponding value of z. If we define

$$\mathbf{R}_t=\bar{\Gamma}\cdot\mathbf{R}'+\mathbf{d}$$

then Z_t is obtained from $g(\mathbf{R}_t)=0$. These quantities are depicted in figure 5. The vectors $\mathbf{R}$ and $\mathbf{R}'$ are given by

$$\mathbf{R}=\mathbf{r}_f+\mathbf{k}\left(\frac{Z-\mathcal{Z}}{k_z}\right) \tag{9}$$

$$\mathbf{R}' = \mathbf{r}_f + \mathbf{k}\left(\frac{Z_t - \mathcal{Z}}{k_z}\right) \tag{10}$$

Using these definitions, the localization conditions are easily written out.

$$\left.\begin{aligned}
\mathcal{Z} &= \frac{\dfrac{\Delta N(\mathbf{R}_t)\nabla_t g(\mathbf{R}_t)\cdot\bar{\Gamma}\cdot\mathbf{K}_x Z_t}{\mathbf{k}\cdot\nabla_t g(\mathbf{R}_t)\cdot\bar{\Gamma}} - \dfrac{\Delta N(\mathbf{R})\nabla g(\mathbf{R})\cdot\mathbf{K}_x Z}{\mathbf{k}\cdot\nabla g(\mathbf{R})}}{\dfrac{\Delta N(\mathbf{R}_t)\hat{\imath}\cdot\nabla_t g(\mathbf{R}_t)\cdot\bar{\Gamma}}{\mathbf{k}\cdot\nabla_t g(\mathbf{R}_t)\cdot\bar{\Gamma}} - \dfrac{\Delta N(\mathbf{R})\hat{\imath}\cdot\nabla g(\mathbf{R})}{\mathbf{k}\cdot\nabla g(\mathbf{R})}} \\
\mathcal{Z} &= \frac{\dfrac{\Delta N(\mathbf{R}_t)\nabla_t g(\mathbf{R}_t)\cdot\bar{\Gamma}\cdot\mathbf{K}_y Z_t}{\mathbf{k}\cdot\nabla_t g(\mathbf{R}_t)\cdot\bar{\Gamma}} - \dfrac{\Delta N(\mathbf{R})\nabla g(\mathbf{R})\cdot\mathbf{K}_y Z}{\mathbf{k}\cdot\nabla g(\mathbf{R})}}{\dfrac{\Delta N(\mathbf{R}_t)\hat{\jmath}\cdot\nabla_t g(\mathbf{R}_t)\cdot\bar{\Gamma}}{\mathbf{k}\cdot\nabla_t g(\mathbf{R}_t)\cdot\bar{\Gamma}} - \dfrac{\Delta N(\mathbf{R})\hat{\jmath}\cdot\nabla g(\mathbf{R})}{\mathbf{k}\cdot\nabla g(\mathbf{R})}}
\end{aligned}\right\} \tag{11}$$

Symbols such as $\nabla_t g(\mathbf{R}_t)$ and $\nabla g(\mathbf{R})$ mean that the differentiations are first performed with respect to $\mathbf{r}_t$ and $\mathbf{r}$ and then the explicit values of $\mathbf{R}$ and $\mathbf{R}_t$ are substituted. To repeat, Z is calculated from $g(R)=0$ and Z_t is calculated from $g(\mathbf{R}_t)=0$. Equations (11) are implicit solutions for the axial localization coordinate $\mathcal{Z}$; hence, additional manipulation is required to obtain $\mathcal{Z}$ as a function of X, Y.

In the next section, the requirements for good localization are discussed qualitatively.

Requirements for Localization

Good localization (sharply defined fringes) will occur when conditions (a), (b), and (c) below are satisfied. Accurate localization (coincidence of interference fringes and shock surface) is promoted by all the conditions (a), (b), (c), and (d).

(a) The view represented by the vector $\mathbf{k}$ is tangential to the shock wave (steep view).

(b) The strength of the shock wave $\Delta N(\mathbf{R})$ varies rapidly enough with position.

(c) The shock wave has sufficient curvature: $g(\mathbf{r})$ contains nonlinear terms in $\mathbf{r}$.

(d) The vector $\mathbf{K}_x$ or $\mathbf{K}_y$ is tangential to the shock wave.

The condition for good localization can be deduced qualitatively by using the results derived above and the results from appendix A.

Recall that the most general condition for localization, obtained from equations (A11), (A17), and (A19), is given by

$$\nabla_r \Delta\theta = \frac{2\pi}{\lambda}\left[\int \nabla_r \mathbf{r}_r \cdot \nabla f \frac{dz}{k_z} + \int \nabla_r \mathbf{k} \cdot \nabla f \frac{z\,dz}{k_z^2}\right] = 0$$

For localization, the phase change $\Delta\theta$ must be stationary with respect to at least one of the components of the position vector $\mathbf{r}_r$ in the reference plane. At the same time, however, the phase change $\Delta\theta$ must depend on that variable if the localization is to be nontrivial. In fact, from equation (A13), the larger that $\nabla_r \Delta\theta$ is at points away from optimum localization, the better localization will be.

Consider only the first component $\hat{\imath}\cdot\nabla_r\Delta\theta$, since the treatment of the second component is identical. Following the same procedure used to derive equations (1) and, thereby, equations (11), it can be shown that

$$\hat{\imath}\cdot\nabla_r\Delta\theta=\frac{2\pi}{\lambda}\left\{\left[\frac{\Delta N(\mathbf{R}_t)\hat{\imath}\cdot\nabla_t g(\mathbf{R}_t)\cdot\bar{\Gamma}}{\mathbf{k}\cdot\nabla_t g(\mathbf{R}_t)\cdot\bar{\Gamma}}-\frac{\Delta N(\mathbf{R})\hat{\imath}\cdot\nabla g(\mathbf{R})}{\mathbf{k}\cdot\nabla g(\mathbf{R})}\right]\right.$$

$$\left.-\frac{1}{\mathcal{Z}}\left[\frac{\Delta N(\mathbf{R}_t)\nabla_t g(\mathbf{R}_t)\cdot\bar{\Gamma}\cdot\mathbf{K}_x Z_t}{\mathbf{k}\cdot\nabla_t g(\mathbf{R}_t)\cdot\bar{\Gamma}}-\frac{\Delta N(\mathbf{R})\nabla g(\mathbf{R})\cdot\mathbf{K}_x Z}{\mathbf{k}\cdot\nabla g(\mathbf{R})}\right]\right\} \tag{12}$$

Note that $\nabla_t g(\mathbf{R}_t)\cdot\bar{\Gamma}$ can be written as $\nabla g(\mathbf{R}_t)$ so that equation (12) can be written as

$$\hat{\imath}\cdot\nabla_r\Delta\theta=\frac{2\pi}{\lambda}\left\{\left[\frac{\Delta N(\mathbf{R}_t)\hat{\imath}\cdot\nabla g(\mathbf{R}_t)}{\mathbf{k}\cdot\nabla g(\mathbf{R}_t)}-\frac{\Delta N(\mathbf{R})\hat{\imath}\cdot\nabla g(\mathbf{R})}{\mathbf{k}\cdot\nabla g(\mathbf{R})}\right]\right.$$

$$\left.-\frac{1}{\mathcal{Z}}\left[\frac{\Delta N(\mathbf{R}_t)\nabla g(\mathbf{R}_t)\cdot\mathbf{K}_x Z_t}{\mathbf{k}\cdot\nabla g(\mathbf{R}_t)}-\frac{\Delta N(\mathbf{R})\nabla g(\mathbf{R})\cdot\mathbf{K}_x Z}{\mathbf{k}\cdot\nabla g(\mathbf{R})}\right]\right\} \tag{13}$$

Equation (13) is composed of pairs of terms. The first term in a pair is evaluated at the intersection of the viewing axis with the second position of the shock wave. The second term in a pair is evaluated at the intersection of the viewing axis with the first position of the shock wave. The general qualitative criterion for good localization (sharply defined fringes) is that the terms in a pair differ significantly. To the lowest order of approximation, $\hat{\imath}\cdot\nabla_r\Delta\theta$ will vary rapidly as $1/\mathcal{Z}$ varies from its value at localization if the multiplier of $1/\mathcal{Z}$ is large. The factors that influence this multiplier are examined one at a time.

The quantity $\mathbf{k}\cdot\nabla g(\mathbf{R})$ is proportional to the inner product of the viewing vector $\mathbf{k}$ and the normal to the shock wave surface $\nabla g(\mathbf{R})/|\nabla g(\mathbf{R})|$. The factor $1/\mathbf{k}\cdot\nabla g(\mathbf{R})$ changes most rapidly as $\mathbf{k}\cdot\nabla g(\mathbf{R})\to 0$. Hence, the two terms in the last bracket in equation (13) will differ most when the view approaches *tangency*. Therefore, a steep view of a shock surface will promote localization.

Conditions (b) and (c) follow fairly easily. The larger the difference between $\Delta N(\mathbf{R}_t)$ and $\Delta N(\mathbf{R})$, the larger will be the multiplier of $1/\mathcal{Z}$. Hence, a large variation in strength as a function of position will promote localization. (Note that the ratio $\Delta N(R)/\Delta N(\mathbf{R}_t)$ will enter the final calculation for $\mathcal{Z}$ as a function of X and Y so that the small absolute values of $\Delta N(\mathbf{R}_t)$ and $\Delta N(\mathbf{R})$ need be of no concern.)

Finally, a large difference between the gradients $\nabla g(\mathbf{R}_t)$ and $\nabla g(\mathbf{R})$ will promote localization. This difference is large if the curvature of the shock surface is large.

Requirements for Accurate Localization

It is desirable that the interference fringes coincide with one of the two positions of the shock wave (accurate localization). In fact, the conditions for good localization (sharp fringes) will yield accurate localization. In addition if $\mathbf{K}_x$ or $\mathbf{K}_y$ is tangential to the shock surface, the localization will be accurate. Conditions (a) to (d) for accurate localization are examined in the light of the first of equations (11).

To manipulate the first of equations (11) effectively, it is convenient to note that

$$\mathbf{K}_x=\hat{\imath}-k_x\mathbf{k} \tag{14}$$

For condition (a), let the view be tangential:

$$\mathbf{k}\cdot\nabla g(\mathbf{R})\to 0$$

Then, from the first of equations (11),

$$\mathcal{Z} = \frac{\nabla g(\mathbf{R}) \cdot K_x Z}{\hat{\imath} \cdot \nabla g(\mathbf{R})} \tag{15}$$

However, from equation (14)

$$\nabla g(\mathbf{R}) \cdot \mathbf{K}_x = \nabla g(\mathbf{R}) \cdot \hat{\imath} - k_x \nabla g(\mathbf{R}) \cdot \mathbf{k} = \nabla g(\mathbf{R}) \cdot \hat{\imath} \tag{16}$$

Substituting this into equation (15), it follows that $\mathcal{Z} = Z$. Then, from equation (9), $\mathbf{R} = \mathbf{r}_f$ and a position on the fringe is also a position on the shock surface. The localization is exact.

For condition (d) let $\mathbf{K}_x \cdot \nabla g(\mathbf{R}) = 0$ so that $\mathbf{K}_x$ is tangential at the shock surface. Then, from the first of equations (11),

$$\mathcal{Z} = \frac{\dfrac{\Delta N(\mathbf{R}_t) \nabla g(\mathbf{R}_t) \cdot \mathbf{K}_x Z_t}{\mathbf{k} \cdot \nabla g(\mathbf{R}_t)}}{\dfrac{\Delta N(\mathbf{R}_t) \hat{\imath} \cdot \nabla g(\mathbf{R}_t)}{\mathbf{k} \cdot \nabla g(\mathbf{R}_t)} - \dfrac{\Delta N(\mathbf{R}) \hat{\imath} \cdot \nabla g(\mathbf{R})}{\mathbf{k} \cdot \nabla g(\mathbf{R})}} \tag{17}$$

Let the strength of the shock wave be the same at both positions $\mathbf{R}$ and $\mathbf{R}'$. (This assumption will allow us to achieve exact localization.) Then,

$$\mathcal{Z} = \frac{\dfrac{\nabla g(\mathbf{R}_t) \cdot \mathbf{K}_x Z_t}{\mathbf{k} \cdot \nabla g(\mathbf{R}_t)}}{\dfrac{\hat{\imath} \cdot \nabla g(\mathbf{R}_t)}{\mathbf{k} \cdot \nabla g(\mathbf{R}_t)} - \dfrac{\hat{\imath} \cdot \nabla g(\mathbf{R})}{\mathbf{k} \cdot \nabla g(\mathbf{R})}} \tag{18}$$

From equation (16) $\nabla g(\mathbf{R}) \cdot \hat{\imath} - k_x \nabla g(\mathbf{R}) \cdot \mathbf{k} = 0$, so that

$$k_x = \frac{\hat{\imath} \cdot \nabla g(\mathbf{R})}{\mathbf{k} \cdot \nabla g(\mathbf{R})}$$

Substituting this expression and equation (14) into equation (18) yields

$$\mathcal{Z} = \frac{\dfrac{\nabla g(\mathbf{R}_t) \cdot [\hat{\imath} - k_x \mathbf{k}]}{\mathbf{k} \cdot \nabla g(\mathbf{R}_t)} Z_t}{\dfrac{\hat{\imath} \cdot \nabla g(\mathbf{R}_t)}{\mathbf{k} \cdot \nabla g(\mathbf{R}_t)} - k_x}$$

$$\mathcal{Z} = Z_t$$

Localization is exact at the second position of the shock wave.

Conditions (b) and (c) do not yield localization as readily. However, it can be seen that these conditions improve localization.

For condition (b) let the strength at $\mathbf{R}'$ ($\mathbf{R}_t$ in the transformed coordinate system) be negligible compared with the strength at $\mathbf{R}$. Then the first of equations (11) becomes

$$\mathcal{Z} = \frac{\nabla g(\mathbf{R}) \cdot \mathbf{K}_x Z}{\hat{\imath} \cdot \nabla g(\mathbf{R})} \tag{19}$$

From equations (14) and (19)

$$\mathcal{Z} = Z - k_x \frac{\mathbf{k}\cdot\nabla g(\mathbf{R})}{\hat{\imath}\cdot\nabla g(\mathbf{R})} \tag{20}$$

If the view is close to being normal to the reference plane ($k_x \approx 0$), then $\mathcal{Z} \approx Z$ and localization is nearly exact.

For condition (c), let $\hat{\imath}\cdot\nabla g(\mathbf{R})$ be very large in comparison with $\hat{\imath}\cdot\nabla g(\mathbf{R}_t)$ (the curvature is large in the x,z plane). Also, let $\Delta N(\mathbf{R}_t) = \Delta N(\mathbf{R})$. Neglecting $\hat{\imath}\cdot\nabla g(\mathbf{R}_t)$, the first of equations (11) becomes

$$\mathcal{Z} = \frac{-k_x Z_t - \dfrac{\nabla g(\mathbf{R})\cdot\mathbf{K}_x Z}{\mathbf{k}\cdot\nabla g(\mathbf{R})}}{-\dfrac{\hat{\imath}\cdot\nabla g(\mathbf{R})}{\mathbf{k}\cdot\nabla g(\mathbf{R})}} \tag{21}$$

On substituting equation (14) into $\nabla g(\mathbf{R})\cdot\mathbf{K}_x$ equation (21) becomes

$$\mathcal{Z} = \frac{-k_x(Z_t - Z) - \dfrac{\hat{\imath}\cdot\nabla g(\mathbf{R})}{\mathbf{k}\cdot\nabla g(\mathbf{R})} Z}{-\dfrac{\hat{\imath}\cdot\nabla g(\mathbf{R})}{\mathbf{k}\cdot\nabla g(\mathbf{R})}} \tag{22}$$

If the difference between Z and Z_t is negligible then $\mathcal{Z} \approx Z$, and localization is nearly exact.

As the view approaches tangency, condition (a) promotes both good and accurate localization. If condition (a) is not satisfied, then a combination of conditions (b), (c), and (d) will probably be required to promote localization.

To determine quantiatively the criteria for good and accurate localization, it is necessary to treat a specific example. The case of a shock wave between the blades of a compressor rotor is examined next.

Rapid-Double-Exposure Holography of An Interblade Shock Wave in a Rotating Compressor

The results from the previous section of this report are applied to a shock wave generated by the blades of a compressor rotor. The motion of the shock wave between exposures is due to the rotation of the compressor. However, the step-by-step application of the fundamentals of fringe localization theory would be the same for any type of shock-wave motion.

The equations for locating the interference fringes are derived subject to the assumption that the compressor rotates through a small angle α between exposures. A localization error is defined, and that definition of localization error is shown to be consistent with the requirements for accurate localization specified in the previous section. By using a polynomial representation of the shock surface, the equations derived are in a form suitable for comparison with actual data.

The first step is to define an appropriate frame of reference.

Reference Frame Relative to a Particular Blade Passage

An interblade passage will be located between the suction surface of the upper blade and the pressure surface of the lower blade defining the passage as shown in figure 6.

The origin of coordinates in figure 6 is arbitrarily chosen at maximum span and at the leading edge of the lower blade defining the passage. From this point the y axis is selected to be parallel to the axis of rotation and to point downstream.

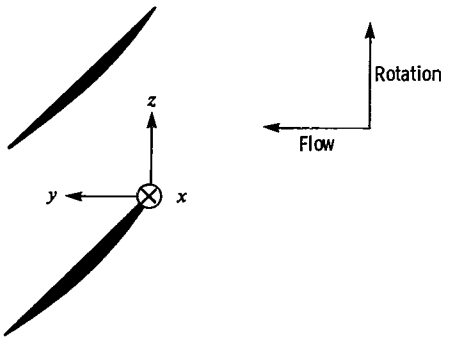

Figure 6. - Blade passage and reference coorinate system in compressor rotor.

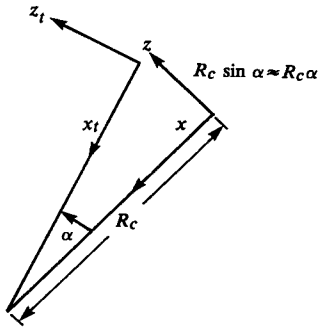

Figure 7. - Translation of coordinates when a compressor rotates through small angle α.

The z axis is tangent to the circumferential circle of the compressor and points in the direction of rotation. Then, for a right-handed coordinate system, the x axis will point radially inward toward the axis of rotation. The next step is to define the appropriate transformation of coordinates.

Transformation of Coordinates at Second Exposure

Between exposures, assume that the compressor rotor rotates through a small enough angle α that only first-order terms in α need be retained at any stage of the calculation. The rotation tensor in equation (4) is then given by

$$\bar{\Gamma} = \bar{\mathbf{E}} + \bar{\Omega}\alpha \tag{23}$$

where $\bar{\mathbf{E}}$ is the identity tensor and

$$\bar{\Gamma} = -\hat{\imath}\hat{k} + \hat{k}\hat{\imath} \tag{24}$$

The translation vector in equation (4) can be derived by referring to the view in the xz plane (fig. 7). The radius of the blades measured from the axis of the compressor is called R_c. The translation vector is given by

$$\mathbf{d} = (0, 0, -R_c\alpha) \tag{25}$$

Substituting equation (23) into equation (4) results in the following coordinates at the second exposure:

$$\mathbf{r}_t = \mathbf{r} + \alpha\bar{\Omega}\cdot\mathbf{r} + \mathbf{d} \tag{26}$$

Representation $g(\mathbf{r}) = 0$ of the Shock Wave

To make comparisons with experimental data easier, the shock wave will be represented by the polynominal

$$g(\mathbf{r}) = z - \sum_i A_i(x)y^i = 0 \tag{27}$$

Note that the coefficients are functions of the x coordinate only. At this point, the problem is one of methodical substitution.

Treatment of Variation in Shock Strength $\Delta N(\mathbf{R})$

Define the ratio of the shock strength at $\mathbf{R}$ to the shock strength at $\mathbf{R}'(\mathbf{R}_t$ in transformed

system) by

$$n = \frac{\Delta N(\mathbf{R})}{\Delta N(\mathbf{R}_t)}$$

Now, assume that $\Delta n = 1 - n$ is a small quantity. Retain only terms of order Δn at any stage of the calculation. To simplify the expansion to first order in Δn and α, equations (11) for localization are rearranged as shown below. Note that terms of order $\alpha \Delta n$ are second order and are ignored.

$$\mathcal{Z} = \frac{\dfrac{\nabla_t g(\mathbf{R}_t)\cdot\bar{\Gamma}\cdot\mathbf{K}_x Z_t}{\mathbf{k}\cdot\nabla_t g(\mathbf{R}_t)\cdot\bar{\Gamma}} - \dfrac{\nabla g(\mathbf{R})\cdot\mathbf{K}_x Z}{\mathbf{k}\cdot\nabla g(\mathbf{R})} + \dfrac{\Delta n\,\nabla g(\mathbf{R})\cdot\mathbf{K}_x Z}{\mathbf{k}\cdot\nabla g(\mathbf{R})}}{\dfrac{\hat{\imath}\cdot\nabla_t g(\mathbf{R}_t)\cdot\bar{\Gamma}}{\mathbf{k}\cdot\nabla_t g(\mathbf{R}_t)\cdot\bar{\Gamma}} - \dfrac{\hat{\imath}\cdot\nabla g(\mathbf{R})}{\mathbf{k}\cdot\nabla g(\mathbf{R})} + \dfrac{\Delta n\hat{\imath}\cdot\nabla g(\mathbf{R})}{\mathbf{k}\cdot\nabla g(\mathbf{R})}}$$

$$\mathcal{Z} = \frac{\dfrac{\nabla_t g(\mathbf{R}_t)\cdot\bar{\Gamma}\cdot\mathbf{K}_r Z_t}{\mathbf{k}\cdot\nabla_t g(\mathbf{R}_t)\cdot\bar{\Gamma}} - \dfrac{\nabla g(\mathbf{R})\cdot\mathbf{K}_y Z}{\mathbf{k}\cdot\nabla g(\mathbf{R})} + \dfrac{\Delta n\,\nabla g(\mathbf{R})\cdot\mathbf{K}_y Z}{\mathbf{k}\cdot\nabla g(\mathbf{R})}}{\dfrac{\hat{\jmath}\cdot\nabla_t g(\mathbf{R}_t)\cdot\bar{\Gamma}}{\mathbf{k}\cdot\nabla_t g(\mathbf{R}_t)\cdot\bar{\Gamma}} - \dfrac{\hat{\jmath}\cdot\nabla g(\mathbf{R})}{\mathbf{k}\cdot\nabla g(\mathbf{R})} + \dfrac{\Delta n\hat{\jmath}\cdot\nabla g(\mathbf{R})}{\mathbf{k}\cdot\nabla g(\mathbf{R})}} \tag{28}$$

Expansion to First Order in α and Δn

On expanding equations (28) to first order in α and Δn, these equations can be written in the form of exact-localization-plus-an-error. This expansion can be followed more easily by accomplishing it in several steps.

First note that the first order in α,

$$Z_t = Z + \left.\frac{dZ_t}{d\alpha}\right|_{\alpha=0}\alpha$$

Substituting this into equations (28) yields

$$\mathcal{Z} = \frac{\left[\dfrac{\nabla_t g(\mathbf{R}_t)\cdot\bar{\Gamma}\cdot\mathbf{K}_x}{\mathbf{k}\cdot\nabla_t g(\mathbf{R}_t)\cdot\bar{\Gamma}} - \dfrac{\nabla g(\mathbf{R})\cdot\mathbf{K}_x}{\mathbf{k}\cdot\nabla g(\mathbf{R})} + \dfrac{\Delta n\,\nabla g(\mathbf{R})\cdot\mathbf{K}_x}{\mathbf{k}\cdot\nabla g(\mathbf{R})}\right]Z + \left[\dfrac{\nabla g(\mathbf{R})\cdot\mathbf{K}_x}{\mathbf{k}\cdot\nabla g(\mathbf{R})}\right]\left.\dfrac{dZ_t}{d\alpha}\right|_{\alpha=0}\alpha}{\dfrac{\hat{\imath}\cdot\nabla_t g(\mathbf{R}_t)\cdot\bar{\Gamma}}{\mathbf{k}\cdot\nabla_t g(\mathbf{R}_t)\cdot\bar{\Gamma}} - \dfrac{\hat{\imath}\cdot\nabla g(\mathbf{R})}{\mathbf{k}\cdot\nabla g(\mathbf{R})} + \dfrac{\Delta n\hat{\imath}\cdot\nabla g(\mathbf{R})}{\mathbf{k}\cdot\nabla g(\mathbf{R})}}$$

$$\mathcal{Z} = \frac{\left[\dfrac{\nabla_t g(\mathbf{R}_t)\cdot\bar{\Gamma}\cdot\mathbf{K}_y}{\mathbf{k}\cdot\nabla_t g(\mathbf{R}_t)\cdot\bar{\Gamma}} - \dfrac{\nabla g(\mathbf{R})\cdot\mathbf{K}_y}{\mathbf{k}\cdot\nabla g(\mathbf{R})} + \dfrac{\Delta n\,\nabla g(\mathbf{R})\cdot\mathbf{K}_y}{\mathbf{k}\cdot\nabla g(\mathbf{R})}\right]Z + \left[\dfrac{\nabla g(\mathbf{R})\cdot\mathbf{K}_y}{\mathbf{k}\cdot\nabla g(\mathbf{R})}\right]\left.\dfrac{dZ_t}{d\alpha}\right|_{\alpha=0}\alpha}{\dfrac{\hat{\jmath}\cdot\nabla_t g(\mathbf{R}_t)\cdot\bar{\Gamma}}{\mathbf{k}\cdot\nabla_t g(\mathbf{R}_t)} - \dfrac{\hat{\jmath}\cdot\nabla g(\mathbf{R})}{\mathbf{k}\cdot\nabla g(\mathbf{R})} + \dfrac{\Delta n\hat{\jmath}\cdot\nabla g(\mathbf{R})}{\mathbf{k}\cdot\nabla g(\mathbf{R})}} \tag{29}$$

Specific use has been made of the fact that

$$\left.\frac{\nabla_t g(\mathbf{R}_t)\cdot\bar{\Gamma}\cdot\mathbf{K}_x}{\mathbf{k}\cdot\nabla_t g(\mathbf{R}_t)\cdot\Gamma}\right|_{\alpha=0} = \frac{\nabla g(\mathbf{R})\cdot\mathbf{K}_x}{\mathbf{k}\cdot\nabla g(\mathbf{R})}$$

and similarly when $\mathbf{K}_x$ is replaced by $\mathbf{K}_y$.

Now, in the first brackets of equations (29), substitute equation (14) for $\mathbf{K}_x$ and a similar equation for $\mathbf{K}_y$.

$$\mathcal{Z} = Z + \frac{\left[\dfrac{\nabla g(\mathbf{R})\cdot\mathbf{K}_x}{\mathbf{k}\cdot\nabla g(\mathbf{R})}\right]\left.\dfrac{dZ_t}{d\alpha}\right|_{\alpha=0}\alpha - k_x Z\Delta n}{\dfrac{\hat{\imath}\cdot\nabla_t g(\mathbf{R}_t)\cdot\bar{\Gamma}}{\mathbf{k}\cdot\nabla_t g(\mathbf{R}_t)\cdot\bar{\Gamma}} - \dfrac{\hat{\imath}\cdot\nabla g(\mathbf{R})}{\mathbf{k}\cdot\nabla g(\mathbf{R})} + \dfrac{\Delta n\hat{\imath}\cdot\nabla g(\mathbf{R})}{\mathbf{k}\cdot\nabla g(\mathbf{R})}}$$

$$\mathcal{Z} = Z + \frac{\left[\dfrac{\nabla g(\mathbf{R})\cdot\mathbf{K}_y}{\mathbf{k}\cdot\nabla g(\mathbf{R})}\right]\left.\dfrac{dZ_t}{d\alpha}\right|_{\alpha=0}\alpha - k_y Z\Delta n}{\dfrac{\hat{\jmath}\cdot\nabla_t g(\mathbf{R}_t)\cdot\bar{\Gamma}}{\mathbf{k}\cdot\nabla_t g(\mathbf{R}_t)\cdot\bar{\Gamma}} - \dfrac{\hat{\jmath}\cdot\nabla g(\mathbf{R})}{\mathbf{k}\cdot\nabla g(\mathbf{R})} + \dfrac{\Delta n\hat{\jmath}\cdot\nabla g(\mathbf{R})}{\mathbf{k}\cdot\nabla g(\mathbf{R})}} \tag{30}$$

Equations (30) are now in the form of exact-localization-plus-an-error. However, the denominator has not yet been expanded.

To expand the denominators of equations (30), the following relationships are used for the first of equations (30) and similar relationships for the second:

$$\frac{\hat{\imath}\cdot\nabla_t g(\mathbf{R}_t)\cdot\bar{\Gamma}}{\mathbf{k}\cdot\nabla_t g(\mathbf{R}_t)\cdot\bar{\Gamma}} = \frac{\hat{\imath}\cdot\nabla g(\mathbf{R})}{\mathbf{k}\cdot\nabla g(\mathbf{R})}\left[1 + \frac{(d/d\alpha)(\hat{\imath}\cdot\nabla_t g(\mathbf{R}_t)\cdot\bar{\Gamma})\big|_{\alpha=0}\alpha}{\hat{\imath}\cdot\nabla g(\mathbf{R})} - \frac{(d/d\alpha)(\mathbf{k}\cdot\nabla_t g(\mathbf{R}_t)\cdot\bar{\Gamma})\big|_{\alpha=0}\alpha}{\mathbf{k}\cdot\nabla g(\mathbf{R})}\right] \tag{31}$$

$$\frac{d}{d\alpha}(\hat{\imath}\cdot\nabla_t g(\mathbf{R}_t)\cdot\bar{\Gamma})\Big|_{\alpha=0} = \hat{\imath}\cdot\nabla g(\mathbf{R})\cdot\bar{\Omega} + \hat{\imath}\cdot\frac{d}{d\alpha}\nabla_t g(\mathbf{R}_t)\Big|_{\alpha=0} \tag{32}$$

$$\frac{d}{d\alpha}(\mathbf{k}\cdot\nabla_t g(\mathbf{R}_t)\cdot\bar{\Gamma})\Big|_{\alpha=0} = \mathbf{k}\cdot\nabla g(\mathbf{R})\cdot\bar{\Omega} + \mathbf{k}\cdot\frac{d}{d\alpha}\nabla_t g(\mathbf{R}_t)\Big|_{\alpha=0} \tag{33}$$

On substituting these relationships and performing some manipulation, equations (30) become

$$\left.\begin{aligned}
\mathcal{Z} = Z + &\left\{\frac{[\mathbf{K}_x\cdot\nabla g(\mathbf{R})][\mathbf{k}\cdot\nabla g(\mathbf{R})](dZ_t/d\alpha)\big|_{\alpha=0}}{[\hat{\imath}\cdot\mathbf{g}(\mathbf{R})]} - \frac{k_x[\mathbf{k}\cdot\nabla g(\mathbf{R})]^2 Z(\Delta n/\alpha)}{[\hat{\imath}\cdot\nabla g(\mathbf{R})]}\right\}\Bigg/ \\
&\left\{\frac{\Delta n}{\alpha}[\mathbf{k}\cdot\nabla g(\mathbf{R})] + \frac{[\mathbf{k}\cdot\nabla g(\mathbf{R})]}{[\hat{\imath}\cdot\nabla g(\mathbf{R})]}\left[\hat{\imath}\cdot\frac{d}{d\alpha}\nabla_t g(\mathbf{R}_t)\Big|_{\alpha=0}\right] - \left[\mathbf{k}\cdot\frac{d}{d\alpha}\nabla_t g(\mathbf{R}_t)\Big|_{\alpha=0}\right]\right. \\
&\left. - [\mathbf{k}\cdot\nabla g(\mathbf{R})\cdot\bar{\Omega}] + \frac{[\mathbf{k}\cdot\nabla g(\mathbf{R})]}{\hat{\imath}\cdot\nabla g(\mathbf{R})}[\hat{\imath}\cdot\nabla g(\mathbf{R})\cdot\bar{\Omega}]\right\} \\
\mathcal{Z} = Z + &\left\{\frac{[\mathbf{K}_y\cdot\nabla g(\mathbf{R})][\mathbf{k}\cdot\nabla g(\mathbf{R})](dZ_t/d\alpha)_{\alpha=0}}{[\hat{\jmath}\cdot\mathbf{g}(\mathbf{R})]} - \frac{k_y[\mathbf{k}\cdot\nabla g(\mathbf{R})]^2 Z(\Delta n/\alpha)}{[\hat{\jmath}\cdot\nabla g(\mathbf{R})]}\right\}\Bigg/ \\
&\left\{\frac{\Delta n}{\alpha}[\mathbf{k}\cdot\nabla g(\mathbf{R})] + \frac{[\mathbf{k}\cdot\nabla g(\mathbf{R})]}{[\hat{\jmath}\cdot\nabla g(\mathbf{R})]}\left[\hat{\jmath}\cdot\frac{d}{d\alpha}\nabla_t g(\mathbf{R}_t)_{\alpha=0}\right] - \left[\mathbf{k}\cdot\frac{d}{d\alpha}\nabla_t g(\mathbf{R}_t)_{\alpha=0}\right]\right. \\
&\left. - [\mathbf{k}\cdot\nabla g(\mathbf{R})\cdot\bar{\Omega}] + \frac{[\mathbf{k}\cdot\nabla g(\mathbf{R})]}{\hat{\jmath}\cdot\nabla g(\mathbf{R})}[\hat{\jmath}\cdot\nabla g(\mathbf{R})\cdot\bar{\Omega}]\right\}
\end{aligned}\right\} \tag{34}$$

If the localization error is defined to be $\mathcal{Z}-Z$, it can be seen that the requirements for accurate localization follow immediately. The localization error vanishes when $\mathbf{k}\cdot\nabla g(\mathbf{R})=0$. If $\Delta n=0$, the localization error also vanishes when $\mathbf{K}_x\cdot\nabla g(\mathbf{R})=0$. If Δn is large, the localization error vanishes for a view normal to the reference plane ($k_x=0$). Large values of the curvature that appear through the derivatives with respect to α reduce the localization error toward zero as will be apparent in the Comparison of Localization Error Predictions section.

The polynomial representation of the shock wave is now substituted.

Localization Error Using a Polynominal Representation of the Shock Wave

When equation (27) is used to represent the shock wave, equations (34) for the localization error become

$$\mathcal{Z}-Z=\frac{\left[(k_y^2+k_z^2)-k_xk_y\frac{e_0}{h_0}+k_xk_z\frac{1}{h_0}\right]\left(1-\frac{k_x}{k_z}h_0-\frac{k_y}{k_z}e_0\right)\frac{dZ_t}{d\alpha}}{\frac{\Delta n}{\alpha}\left(1-\frac{k_x}{k_z}h_0-\frac{k_y}{k_z}e_0\right)+\frac{1}{h_0}\frac{dh}{d\alpha}\left(1-\frac{k_y}{k_z}e_0\right)+\frac{k_y}{k_z}\frac{de}{d\alpha}-\frac{1}{h_0}\left(1-\frac{k_y}{k_z}e_0\right)-h_0}$$

$$+\frac{\frac{k_xk_z}{h_0}Z\left(1-\frac{k_y}{k_z}e_0-\frac{k_x}{k_z}h_0\right)^2\frac{\Delta n}{\alpha}}{\frac{\Delta n}{\alpha}\left(1-\frac{k_x}{k_z}h_0-\frac{k_y}{k_z}e_0\right)+\frac{1}{h_0}\frac{dh}{d\alpha}\left(1-\frac{k_y}{k_z}e_0\right)+\frac{k_y}{k_z}\frac{de}{d\alpha}-\frac{1}{h_0}\left(1-\frac{k_y}{k_z}e_0\right)-h_0} \tag{35}$$

$$\mathcal{Z}-Z=\frac{\left[(k_x^2+k_z^2)-k_xk_y\frac{h_0}{e_0}+k_yk_z\frac{1}{e_0}\right]\left(1-\frac{k_x}{k_z}h_0-\frac{k_y}{k_z}e_0\right)\frac{dZ_t}{d\alpha}}{\frac{\Delta n}{\alpha}\left(1-\frac{k_x}{k_z}h_0-\frac{k_y}{k_z}e_0\right)+\frac{1}{e_0}\frac{de}{d\alpha}\left(1-\frac{k_x}{k_z}h_0\right)+\frac{k_x}{k_z}\frac{dh}{d\alpha}-\frac{k_x}{k_z}-h_0}$$

$$+\frac{\frac{k_yk_z}{e_0}Z\left(1-\frac{k_y}{k_z}e_0-\frac{k_x}{k_z}h_0\right)^2\frac{\Delta n}{\alpha}}{\frac{\Delta n}{\alpha}\left(1-\frac{k_x}{k_z}h_0-\frac{k_y}{k_z}e_0\right)+\frac{1}{e_0}\frac{de}{d\alpha}\left(1-\frac{k_x}{k_z}h_0\right)+\frac{k_x}{k_z}\frac{dh}{d\alpha}-\frac{k_x}{k_z}-h_0} \tag{36}$$

where the evaluation of derivatives at $\alpha=0$ is no longer shown explicitly and where equations (35) and (36) are obtained from equations (34) using the following definitions and relationships.

At the intersection of the viewing axis with the first position of the shock wave (position **R** in fig. 5), the normal to the shock surface is given by

$$\nabla g(\mathbf{R})=(-h_0,\ -e_0,\ 1)$$

where

$$h_0=\sum_i\frac{\partial}{\partial x}A_i[\hat{\imath}\cdot\mathbf{R}][\hat{\jmath}\cdot\mathbf{R}]^i$$

is the slope in planes parallel to the xz plane and where

$$e_0=\sum_i iA_i[\hat{\imath}\cdot\mathbf{R}][\hat{\jmath}\cdot\mathbf{R}]^{i-1} \tag{37}$$

is the slope in planes parallel to the yz plane. Both e_0 and h_0 are obtained from the polynominal representation of the shock wave (eq. (27)).

At the intersection of the viewing axis with the second position of the shock wave (position $\mathbf{R}'$ in fig. 5 or $\mathbf{R}_t$ in the transformed coordinate system), the change in normal is obtained to first order from the derivative of the normal with respect to the rotation angle. This derivative is evaluated subject to the constraint that the intersection points lie on the viewing axis. The derivative of the normal is given by

$$\frac{d}{d\alpha}\nabla_t g(\mathbf{R}_t)=\left(-\frac{dh}{d\alpha},-\frac{de}{d\alpha},1\right)$$

where h and e are the slopes h_0 and e_0 evaluated at the intersection of the viewing axis with the second position of the shock wave and where h and e are expressed in the transformed coordinate system. The derivatives of these slopes at $\alpha=0$ are given by

$$\frac{dh}{d\alpha}=\sum_i \frac{\partial^2}{\partial x^2}A_i[\hat{\imath}\cdot\mathbf{R}][\hat{\jmath}\cdot\mathbf{R}]^i\left[\frac{k_x}{k_z}\frac{dZ_t}{d\alpha}-Z\right]+\sum_i i\frac{\partial}{\partial x}A_i[\hat{\imath}\cdot\mathbf{R}][\hat{\jmath}\cdot\mathbf{R}]^{i-1}\frac{k_y}{k_z}\frac{dZ_t}{d\alpha} \tag{38}$$

$$\frac{de}{d\alpha}=\sum_i i\frac{\partial}{\partial x}A_i[\hat{\imath}\cdot\mathbf{R}][\hat{\jmath}\cdot\mathbf{R}][\hat{\jmath}\cdot\mathbf{R}]^{i-1}\left[\frac{k_x}{k_z}\frac{dZ_t}{d\alpha}-Z\right]+\sum_i i(i-1)A_i[\hat{\imath}\cdot\mathbf{R}][\hat{\jmath}\cdot\mathbf{R}]^{i-2}\frac{k_y}{k_z}\frac{dZ_t}{d\alpha} \tag{39}$$

The quantity $dZ_t/d\alpha$ can be evaluated from $g(\mathbf{R}_t)=0$ and $d/d\alpha\, g(\mathbf{R}_t)=\nabla g(\mathbf{R})\cdot d\mathbf{R}_t/d\alpha=0$ and is given by

$$\frac{dZ_t}{d\alpha}=\frac{R_c-h_0Z-\hat{\imath}\cdot\mathbf{R}}{1-(k_x/k_z)h_0-(k_y/k_z)e_0} \tag{40}$$

$$\hat{\imath}\cdot\mathbf{R}=\mathrm{X}+\frac{k_x}{k_z}(Z-\mathcal{Z})$$

$$\hat{\jmath}\cdot\mathbf{R}=\mathrm{Y}+\frac{k_y}{k_z}(Z-\mathcal{Z}) \tag{41}$$

Final Comments on Localization Equations (34), or (35) and (36)

Three facts should be kept in mind in using the localization equations: (1) Although the localization error has been defined as $\mathcal{Z}-Z$, the actual error is the distance along the viewing axis between the first position of the shock wave and the interference fringes and is given by the vector $(\mathcal{Z}-Z)\mathbf{k}/k_z$, where the viewing axis is assumed to intersect the shock wave only once during each exposure. In the limit of tangency at a plane shock wave, this assumption is violated, making this singular case harder to handle. However, if the localization error is redefined as the actual distance between the fringe and the shock wave measured along the z axis, the redefined localization error is well behaved and satisfies the previously stated requirements for accurate localization. Here, it must be kept in mind that a point on the shock wave is still associated with a point on the interference fringes via the viewing vector $\mathbf{k}$.

In this section, exact localization is said to occur when $\mathcal{Z}=Z$. Actually, the two positions of the shock wave are indistinguishable as a result of using expansions to order α only. The residual error is of order αR_c.

In the next section, the theory in this section is compared with measurements from laser anemometry and holography.

Comparison of Localization Error Predictions with Holographic and Laser Anemometer Measurements in a Transonic Compressor Rotor

Rapid-double-exposure holograms were recorded in a compressor rotor at Lewis. Earlier, laser anemometry had been used to measure the velocity between the blades of the same compressor (ref. 1). Among those flow conditions recorded holographically were the same conditions that had been mapped by anemometry. Hence, anemometer data are used in this report as a basis for a calculation of localization error.

A previous report (ref. 10) displays the anemometer measurements of the positions of the passage-shock and bow waves at the choke, or maximum-flow, condition of the compressor stage. At that same condition, the position of the corresponding fringe measured from a rapid-double-exposure hologram was shown for comparison. The figure from that report is reproduced herein as figure 8. However, this report treats instead a hologram recorded near the stall condition of the compressor at 100 percent speed. Laser anemometer data are available at that flow condition also, and the localization error is larger. Figure 4 shows the flow condition reported in this section.

The important features of recording rapid-double-exposure holograms in the Lewis compressor are described next.

Recording the Hologram

Rapid-double-exposure holograms were recorded using the equipment and setup described

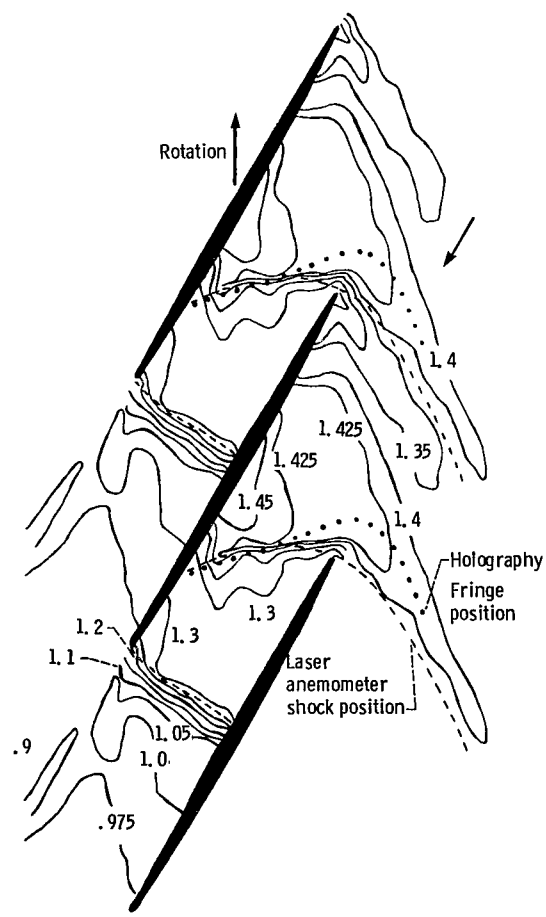

Figure 8. - Laser anemometer and holographic data at choke.

under the Background section. More than 200 holograms were recorded of flow conditions ranging from choke to stall and compressor speeds ranging from 75 to 100 percent of design.

The holograms were recorded on 105-millimeter-film coated with Kodak SO 173 holographic emulsion. This emulsion is sensitive at a wavelength of 694 nanometers, the wavelength radiated by the ruby laser. The film was contained in and advanced by a film transport. A total energy of about 200 millijoules was radiated by the laser in recording a hologram.

Once the compressor test section was constructed and the holocamera was erected, only three parameters could be controlled: the energy radiated by the laser, the time of firing of the laser, and the time between exposures. The laser was fired either at random or by the electronic shaft angle encoder mentioned in the Background section. Since at least two full blade passages appeared in any hologram, the time of firing was not particularly important subject to the assumptions of steady flow and no passage-to-passage variation in flow.

The only restriction on the time between exposures is that it be large enough to produce a fringe having a gray level recognizably different from the background gray level. In fact, it is desirable that the time between exposures be as small as possible. Both the effect of window motion and residual localization error of order αR_c are reduced by keeping the time separation small.

For a particular gray level, the time between exposures can be reduced by viewing a shock wave closer to tangency. The, the optical path difference between exposures is increased. Viewing the shock wave close to tangency also reduces the localization error and sharpens the interference fringes. The time between exposures varied from 8 to 12 microseconds. The stall condition was recorded at a time between exposures of 9 microseconds. This time separation can be compared with a separation between 2 and 5 microseconds used to record the holograms reported in reference 2. In that study a more nearly tangent view was easier to achieve for some of the shock waves.

When developed, the holograms were subjected to a measurement procedure.

Measurement of the Fringe Position in the Reconstructed Image

The holograms were reconstructed using a helium-neon laser with a wavelength of 633 nanometers. It is prudent to be aware of three effects in performing this reconstruction: First, the change in wavelength from 694 nanometers (ruby laser) to 633 nanometers (HeNe laser) introduces magnification factors and aberrations. Second, the blades of the compressor, relative to which the fringe position is to be measured, appear only in silhouette. Because of blade motion, light reflected from the blades does not produce a hologram. Third, the flow field was observed through a window having complex curvature. The viewing window, therefore, produces distortion.

The procedure for measuring the fringes in the presence of these effects follows, in part, a procedure in reference 2. The actual compressor rotor (fig. 9) was erected vertically on a table. The reconstruction source and hologram were set up on the same table. The relative positions of the reference source, compressor blades, and hologram had been measured in the test rig. The analysis of appendix B was then applied. The compressor disk, hologram, and reconstruction source were positioned so as to obtain approximately unity longitudinal magnification of the reconstructed image and superposition of that image on the compressor blades. The hologram was then reconstructed, and the compressor and hologram adjusted so as to superimpose the hologram image as closely as possible on the correct blade passages and to obtain as nearly as possible unity magnification at the blade tips. The primary component of the measurements was in the longitudinal direction. Hence, unity magnification in this direction was emphasized. As argued in appendix B, the position error in the transverse direction is consequently 5 percent or less. It was observed that the distortion introduced by the windows was a greater effect. The effect of the wavelength change is subsequently ignored.

To measure the position of the interference fringe, an XYZ translation table was set up with a pointer attached. The pointer was an optical fiber held rigidly at one end and illuminated at the other end. The rigidly held end appeared as a point light source that could be placed in coincidence with the interference fringe.

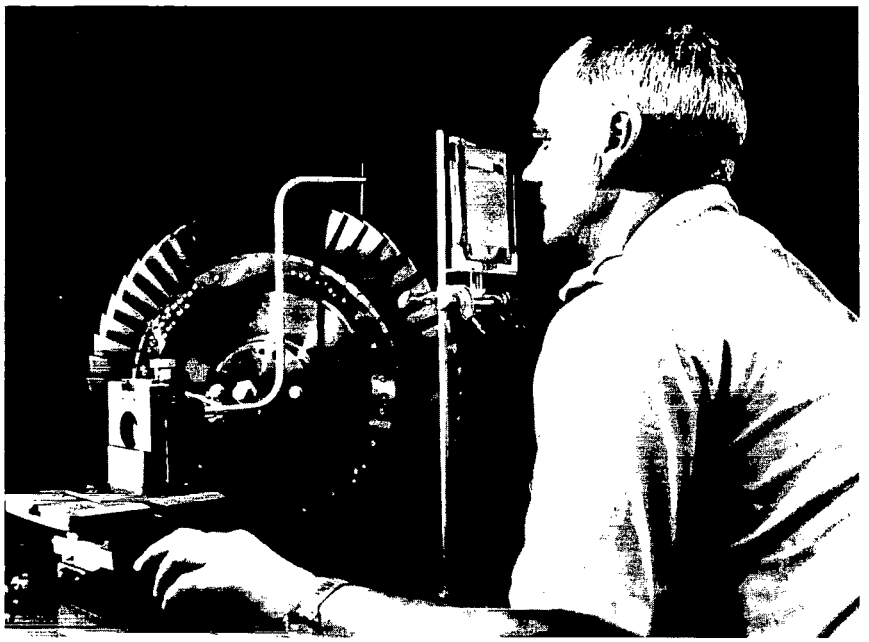

Figure 9. - Compressor rotor and setup for measuring the locations of interference fringes.

The pointer was placed against the leading edge of the lower blade of the passage of interest and at the blade tip. The XYZ translation table was then tilted so that when the Z-axis adjustment alone was advanced, the pointer would travel to the leading-edge tip of the upper blade of the passage of interest. The y axis travel was then parallel to the compressor axis, and the x-axis travel was in the radial direction. The distance indicators were set at (0,0,0) at the leading edge tip of the lower blade of the passage of interest. This arrangement (fig. 10) agrees with the convention in the rest of the paper.

Recognizing that fringe localization is a strong function of viewing direction, some effort was made to restrict the viewing direction for a set of measurements. The plane of the hologram was nearly perpendicular to the table on which the measurements were made. Masks, each containing a horizontal slit (parallel to the table) of width approximately 1 centimeter, were constructed. A mask was taped to the hologram before the measurement of fringe position was made. There was no effect to restrict the eyes (binocular viewing) to a particular position in the horizontal direction. However for the best fringe localization, the hologram tended to be viewed from the center of the slit to the left edge of the slit. For the mask used for the measurements reported in this section, the direction cosines of the viewing vectors to the center and left edge of the mask are listed in table I. The viewing axis is assumed to extend from the origin of the reference coordinate system.

The following procedure was used to measure a fringe. The pointer was set at a particular value of the radial coordinate X. For the measurements reported in this section, $X=0$ (blade tip). The y coordinate (parallel to the compressor axis) was then set at a value beginning at one end of the measurement range. This range extended from about -1.3 to 1.3 centimeters. After setting the y coordinate and while viewing the reconstructed image, the z coordinate alone was varied until the pointer coincided with the fringe. The z coordinate was then recorded. The y coordinate was then stepped to a new position, and the procedure repeated until the measurement range had been scanned. The scan was repeated at least five times for a fringe. The interference fringe was not necessarily detectable or localizable at all values of y.

Fringe Position at 100 Percent Speed Near Stall

The averaged values of the scans at the stall condition are tabulated in table II. The same values are plotted in figure 10. A second-order least-mean-square-error curve fit to the averaged

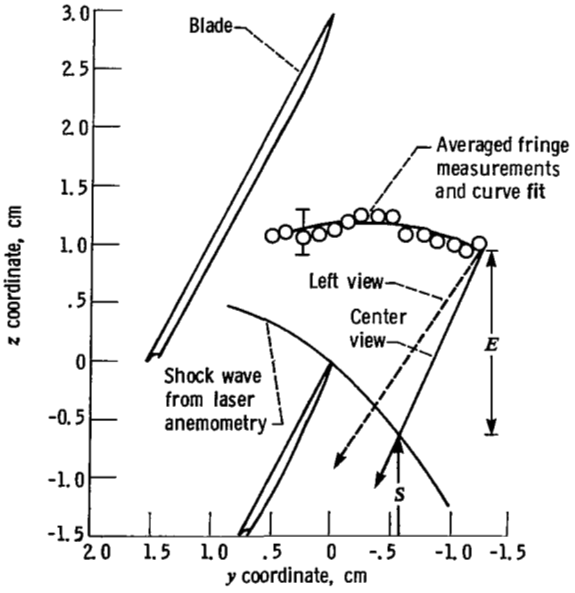

Figure 10. - Shock wave near 100 percent stall measured by laser anemometry together with corresponding fringe from double-exposure holography. Localization error E and shock position S corresponding to one point on the fringe are shown for an assumed center view.

TABLE I.—DIRECTION COSINES FOR MEASUREMENT OF FRINGE POSITION

From mask	k_x	k_y	k_z
Center	−0.436	0.356	−0.826
Left edge	−.416	.495	−.763

TABLE II.—MEASURED POSITION OF INTERFERENCE FRINGE NEAR 100 PERCENT STALL

Y, cm	Z, cm	σ_z, cm
0.508	1.090	0.18
.381	1.110	.19
.254	1.118	.20
.127	1.128	.20
.000	1.173	.21
−.127	1.196	.21
−.254	1.217	.25
−.381	1.219	.25
−.508	1.204	.27
−.635	1.161	.27
−.762	1.105	.28
−.889	1.082	.28
−1.016	1.054	.29
−1.143	1.001	.27
−1.270	.970	.27

data is also plotted in figure 10. The maximum standard deviation of the measurements occurs at $Y = -1.02$ centimeters and is given by $\sigma = 0.28$ centimeter. Also shown in figure 10 is the position of the shock wave measured by laser anemometry.

The shock wave for $Y<0$ is called the bow wave and the shock wave for $Y>0$ is called the passage shock wave.

Assuming that anemometry yields the correct position of the shock wave, the localization error is clearly substantial. Using the anemometer data as a reference, the calculated and measured localization errors are now compared.

Measured Localization Error

First recall the definitions. Referring to figure 10, a point on the interference fringe is designated by the coordinate pair $(Y,\mathcal{Z})$. From that point on the interference fringe, the projection of the viewing axis in the yz plane is followed back to where it intersects the shock wave (assumed to be given by the laser anemometer data). For one point on the fringe, the projection of the viewing axis to the center of the mask is shown in figure 10 by the solid line, and the projection to the left edge of the masked is shown by the broken line.

The coordinates of the point of intersection of the viewing axis and the shock wave are designated by the coordinate pair $[Y+k_y/k_z(Z-\mathcal{Z}),\ Z]$. Hence, the point on the shock wave having this coordinate pair "causes" the interference fringe at the point $(Y,\mathcal{Z})$.

The localization error is a vector having a magnitude equal to the length of the line segment connecting the points on the shock wave and the fringe. The component of this vector in the z direction is $\mathcal{Z}-Z$, and the component in the y direction is $k_y/k_z(\mathcal{Z}-Z)$. Since these two components are both proportional to $E=\mathcal{Z}-Z$, only that component will be measured and called the "localization error."

Table III lists the measured localization error $E=\mathcal{Z}-Z$ and the y coordinate of intersection of the viewing axis with the shock wave given by

$$S=Y+\frac{k_y}{k_z}(Z-\mathcal{Z})$$

as functions of the y coordinate of the intersection of the viewing axis with the fringe designated by Y. This tabulation is done for k_y/k_z corresponding to the center of the mask and k_y/k_z corresponding to the left edge of the mask. The measured localization error E is plotted also as a function of S in figure 11.

For comparison with the localization theory, the localization error is calculated next.

Calculated Localization Error

For this calculation of the localization error, it is assumed that all derivatives in the x direction can be neglected. Then equation (36) is employed with $h_0=0$ and $dh/d\alpha=0$. It is also assumed that the variation in shock-wave strength with position can be neglected so that $\Delta n=0$. Finally, a polynominal representation to fifth order of the anemometer measurement of the shock wave is used:

$$Z=\sum_{i=0}^{5} A_i S^i$$

The coefficients of this expression are listed in table IV.

TABLE III.—MEASURED LOCALIZATION ERROR FOR TWO VIEWING VECTORS

(a) Center			(b) Left edge		
Y, cm	S, cm	E, cm	Y, cm	S, cm	E, cm
−1.27	−0.58	1.59	−1.27	−0.38	1.32
−1.016	−.38	1.45	−1.016	−.20	1.24
−.762	−.20	1.32	−.762	0	1.14
−.508	0	1.17	−.508	.18	1.04
−.254	.23	1.02	−.254	.36	.94
0	.41	.94	0	.53	.81
.254	.58	.79	.254	.71	.66
.508	.79	.64	.508	.89	.58

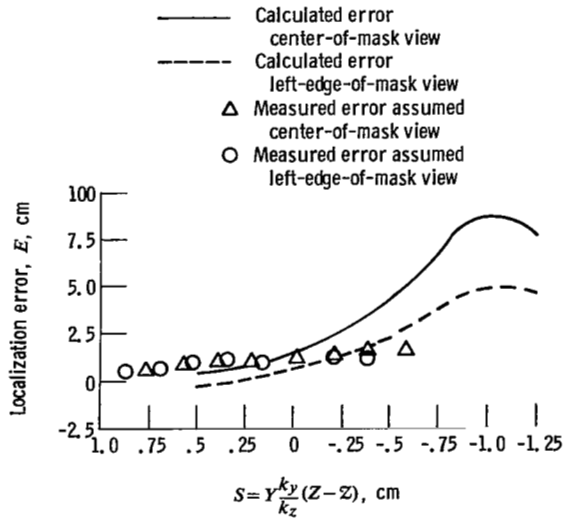

Figure 11. - Measured and calculated localization error E as function of S.

TABLE IV.—COEFFICIENTS IN POLYNOMINAL REPRESENTATION OF SHOCK WAVE DETERMINED BY LASER ANEMOMETRY

A_0	0 cm
A_1	.837
A_2	$-.476\ \text{cm}^{-1}$
A_3	$.01074\ \text{cm}^{-2}$
A_4	$.1051\ \text{cm}^{-3}$
A_5	$.04418\ \text{cm}^{-4}$

When this polynomial is substituted into equation (36) subject to the assumptions, the localization error is given by

$$E = \mathcal{Z} - Z = \frac{\left[(k_x^2 + k_z^2)e_0 + k_y k_z\right]\left(1 - \frac{k_y}{k_z}e_0\right)}{\frac{k_y}{k_z}\sum_{i=2}^{5} i(i-1)A_i S^{i-2} - \frac{\frac{k_x}{k_z}e_0\left(1 - \frac{k_y}{k_z}e_0\right)}{R_c}} \tag{42}$$

where, because of the large value of R_c, equation (40) is written approximately as

$$\left.\frac{dZ_t}{d\alpha}\right|_{\alpha=0} \approx \frac{R_c}{1 - \frac{k_y}{k_z}e_0}$$

Also, note that equation (37) becomes

$$e_0 = \sum_{i=1}^{5} iA_i S^{i-1}$$

The various factors that determine the localization error together with the localization error and the coordinate Y on the interference fringe are listed as functions of S for a viewing vector to the center of the mask in table V. The same quantities are listed in table VI for the viewing vector to the left edge of the mask.

For the two viewing vectors, the localization error is plotted as a function of S in figure 11, which also shows the measured localization error.

Discussion of Results

Referring to figure 11, the agreement between experiment and theory is seen to be good quantitatively and qualitatively. Tables V and VI show clearly what factors influence localization in this application.

First consider figure 11. Depending on the viewing vector, the fringe corresponds to that part of the shock wave extending in the y direction from about $S=-0.5$ to 0.9 centimeter. The agreement between the measured and calculated localization errors is particularly good if it is recalled from appendix A that the fringe is sharpest when the localization error is a minimum. Hence, the eye ought to be attracted to the view that minimizes the localization error. The fringe formed by the bow wave ($S<0$) is sharpest and most easily located when viewed toward the left edge of the mask, and the fringe formed by the pasage shock wave ($S>0$) is sharpest and most easily located when viewed toward the center of the mask or to the right of center. Hence, the broken curve probably represents the localization error when $S<0$, and the solid curve probably represents the localization error when $S>0$. If that is true, then the circles represent the measurements when $S<0$, and the triangles represent the measurements when $S>0$.

It is notable that the fringe corresponding to the bow wave becomes unlocalizable where the calculated localization error starts to increase rapidly. (For the left view, about $S=-0.4$ cm corresponding to $Y=-1.3$ cm on the fringe.)

It is also notable that a singularity in the calculation for the localization error occurs at about $S=0.6$ centimeter. In equation (42) the singularity occurs when the effect of curvature

$$\frac{k_y}{k_z}\sum_{i=2}^{5} i(i-1)S^{i-2}$$

and the effect of rotation

$$\frac{\frac{k_y}{k_z}e_0\left(1-\frac{k_y}{k_z}e_0\right)}{R_c}$$

just cancel.

The calculated location of this singularity is subject to considerable uncertainty for several reasons. The calculation depends on the second derivative of the laser anemometer data, and those data are less accurate in this region. The quantities that were neglected in performing the calculation of localization error (derivatives with respect to x and the variation of shock strength) may have a significant effect on the location of the singularity. Therefore, the fact that the interference fringe disappears about 0.3 centimeter closer to the blade than the calculation indicates is not considered to be significant.

TABLE V.—CALCULATED LOCALIZATION FACTORS FOR VIEW DEFINED BY CENTER OF MASK AND ORIGIN OF REFERENCE FRAME

Position on shock, S, cm	$-\mathbf{K}_y\cdot\nabla g$, $(k_x^2+k_z^2)e_0+k_yk_z$	$\frac{\mathbf{k}\cdot\nabla g}{k_z}$, $1-\frac{k_y}{k_z}e_0$	$\frac{k_y}{k_z}\times$curvature, $\frac{k_y}{k_z}\sum_{i=2}^{5} i(i-1)A_iS^{i-2}$, cm^{-1}	Effect of rotation, $\frac{\frac{k_x}{k_z}e_0\left(1-\frac{k_y}{k_z}e_0\right)}{\mathbf{R}_c}$, cm^{-1}	Position on fringe, Y, cm	Localization error, E, cm
−1.27	1.29	1.78	0.350	0.0669	−4.78	8.13
−1.02	1.13	1.70	.276	.0575	−4.80	8.79
−.762	.988	1.63	.285	.0496	−3.71	6.83
−.508	.829	1.56	.334	.0417	−2.67	4.42
−.254	.643	1.46	.388	.0326	−1.39	2.64
0	.436	1.36	.409	.0236	−.663	1.54
.254	.234	1.26	.361	.0158	−.114	.853
.508	.0827	1.19	.206	.0107	−.290	.505

TABLE VI.—CALCULATED LOCALIZATION FACTORS FOR VIEW DEFINED BY LEFT EDGE OF MASK AND ORIGIN OF REFERENCE FRAME

Position on shock, S, cm	$-\mathbf{K}_y \cdot \nabla g$, $(k_x^2+k_z^2)e_0+k_yk_z$	$\frac{\mathbf{k}\cdot\nabla g}{k_z}$, $1-\frac{k_y}{k_z}e_0$	$\frac{k_y}{k_z}\times$curvature, $\frac{k_y}{k_z}\sum_{i=2}^{5} i(i-1)A_iS^{i-2}$, cm^{-1}	Effect of rotation, $\frac{\frac{k_x}{k_z}e_0\left(1-\frac{k_y}{k_z}e_0\right)}{\mathbf{R}_C}$, cm^{-1}	Position on fringe, Y, cm	Localization error, E, cm
−1.27	0.990	2.18	0.528	0.0689	−4.32	4.70
−1.02	.854	2.06	.417	.0594	−4.22	4.93
−.762	.732	1.95	.429	.0512	−3.22	3.78
−.508	.594	1.84	.504	.0429	−2.05	2.37
−.254	.434	1.70	.587	.0337	−1.12	1.33
0	.254	1.54	.618	.0244	−.427	0.658
.254	.0788	1.39	.543	.0163	.119	.208
.508	−.0518	1.28	.309	.0110	.653	−.222

From tables V and VI, it can be seen that the localization error is kept small as it is by a combination of enough curvature and a sufficiently small value of the inner product

$$(k_x^2+k_z^2)e_0-k_xk_yh_0+k_yk_z=-\mathbf{K}_y\cdot\nabla g(\mathbf{R})$$

(The term $k_xk_yh_0$ has been added back in for reference.)

Incidentally, the superior agreement between the holographic data and the laser anemometer data shown in the blade passage for choke flow (fig. 8) can be attributed to a combination of larger values of curvature and smaller values of $\mathbf{K}_y\cdot\nabla g(\mathbf{R})$ that are calculated for this flow condition.

Conclusions and Recommendations

The theory of fringe localization developed in this report was supported by the holographic and the laser anemometer measurements obtained in the single-stage compressor rig at the Lewis Research Center. The theory shows that there will be a localization error and that it may be large. The presence and value of the error will depend on the curvature of the shock wave, its variation in strength, and its orientation relative to the viewing direction, The only factor that can be controlled to some extent is the viewing direction. If there is some curvature, the localization error can probably be kept small by restricting the view to within plus or minus 30° of tangency to the shock surface. When the view is restricted so that this degree of tangency cannot be achieved, other optical methods of measurement should be considered before rapid-double-exposure holography is attempted.

In any case one may be confronted with fluctuating flows that are not two dimensional or must be examined through windows of low quality or complex curvature. Then, rapid-double-exposure holography is worth trying.

The reasonable way to handle localization error is to avoid it. Using a number of views in an attempt to invert the localization equations seem like a formidable and not very accurate procedure, although this possibility has not been examined in any detail.

The first step in avoiding localization error is to ascertain the available range of the viewing vectors and to estimate the expected range of shapes and orientations of the shock wave. The next step for each orientation of the shock wave is to determine whether there is a viewing axis where the view is close to being tangent to the shock surface. Then the chance for good and accurate localization is excellent. Even if the fringes do not localize accurately for all views, the fact that sharp fringes and accurate localization go together should guide the eye in picking out the best location of the fringe. An additional benefit is that the time between exposures required

to achieve an adequate gray level will also be minimized, thereby minimizing the residual localization error.

If localization is not found to be established by the range of views, it can only be hoped that the shock wave has very strong curvature or a large positional variation in strength or is rotated sharply about an axis near the point of interest. Then the localization error may be acceptably small even though the view is not an optimum view.

Lewis Research Center
National Aeronautics and Space Administration
Cleveland, Ohio, May 1, 1981

Appendix A
Theory of Double-Exposure Holography for Diffuse Illumination of a Time Varying Phase Object

With minor modifications, this theory is based on a treatment by Vest (ref. 8, p. 284–295). Some assumptions will be examined a bit more carefully than in reference 8.

The region of interest is located between a diffuser and a photographic plate or film on which the hologram is recorded (see fig. 12). That region (for this analysis) contains objects that change only the phase of the light passing through them. The objects will include lenses and windows as well as a fluid whose density field is changing in time.

In the region of interest, a plane to be called the reference plane is selected. However, unlike in Vest's treatment, it will be convenient to refer to a reference plane other than the plane of the system diffuser. It will be shown that no complications result if it is assumed that only one ray from any point on the diffuser passes through a point on the reference plane. A coordinate system is erected with its origin and x,y axes in the reference plane. The z axis is then perpendicular to the reference plane.

Now, it is convenient to follow a generally curved light ray from the diffuser through the arbitrary phase object to a point $\mathbf{r}_r \equiv (x,y,0)$ on the reference plane. As stated above, it is assumed that only one light ray from each diffuser point passes through $\mathbf{r}_r$. The ray designated by the symbol S in figure 12 is then continued to an arbitrary point whose coordinates are designated by $\mathbf{r}_f \equiv (X,Y,Z)$. Finally, the ray passes through the plane containing the photographic film and is incident on the aperture of an imaging system. That system could be the eye, a film camera, or a television camera, for example. The reconstructed image and actual phase object will be treated as identical. Thus, there is no distinction between rays that actually pass through the region of interest and rays that are reconstructed in the virtual image of the hologram. The complication of recording and reconstructing the hologram with different wavelengths is treated in appendix B. In figure 12 several curved rays are shown passing through $\mathbf{r}_f$ before they are intercepted by the imaging system. No more than one ray per diffuser point is shown passing through a point on the reference plane. Subject to this contraint, the reference plane is quite arbitrary.

Because the rays are generally curved, there is no guarantee that the point $\mathbf{r}_f$ can be imaged by the lens. In fact, in the most general case, all that can be said is that the rays satisfy the equation

$$\frac{d}{ds}\left(n\frac{d\mathbf{r}}{ds}\right) = \nabla n \tag{A1}$$

where s is the distance along a ray path, where $\mathbf{r}$ is the position of a point on a ray path, and where n is the refractive index at position $\mathbf{r}$. A solution of this equation requires knowing the refractive index n as a function of $\mathbf{r}$. However, the flow visualization methods designed to measure $n(\mathbf{r})$ require knowing the ray paths. For a discussion of this generally intractable problem relevant to Mach-Zehnder interferometry, refer to the fundamental reference by Howes and Buchele (ref. 11).

The only practical approach is to assume simplified functional forms for the ray paths. The assumption in this paper is that the rays are straight lines in the region between the reference

plane and the hologram. This so-called "refractionless limit" can be compromised by anyone of the following effects:

(a) The windows, which may refract the rays

(b) Gradients of refractive index in the fluid, which also may refract the rays, introducing distortion

(c) Gradients of refractive index, which may cause rays to appear to intersect, or to intersect, at $\mathbf{r}_f$ when the intersection would not have occurred in the refractionless limit.

These effects are neglected in the following analysis. The imaging of the rays through $\mathbf{r}_f$ is shown schematically in figure 13 for the holocamera configuration of figure 2.

The electromagnetic field at the image point shown in figure 13 is treated as a summation of scalar expressions having the form

$$U(\mathbf{r}_f;\mathbf{r}_r) = A(\mathbf{r}_f;\mathbf{r}_r)e^{j\varphi(\mathbf{r}_f;\mathbf{r}_r)} \tag{A2}$$

In equation (A2), the vector pair $(\mathbf{r}_f;\mathbf{r}_r)$ defines a particular ray S and, as assumed above, a unique point on the diffuser.

The factor $A(\mathbf{r}_f;\mathbf{r}_r)$ represents the magnitude associated with a ray $\mathbf{r}_f - \mathbf{r}_r$. The factor $e^{j\varphi(\mathbf{r}_f;\mathbf{r}_r)}$ represents the total phase of this ray accumulated in passing from the diffuser to the aperture of the imaging system. The magnitude A contains any radiometric angle factors.

The total field at the image point when the imaging system is focused on $\mathbf{r}_f$ is given by

$$U(\mathbf{r}_f) = \int\int u(\mathbf{r}_f;\, \mathbf{r}_r)d\mathbf{r}_r \tag{A3}$$

The integral is evaluated over that part of the reference plane subtended by the limiting aperture of the imaging system.

It is convenient to represent the phase φ by a sum of phases

$$\varphi(\mathbf{r}_f;\, \mathbf{r}_r) = \varphi_{DI}(\mathbf{r}_f;\, \mathbf{r}_r) + \varphi_{DR}(\mathbf{r}_f;\, \mathbf{r}_r) + \varphi_0(\mathbf{r}_f;\, \mathbf{r}_r) + \varphi_F(\mathbf{r}_f;\, \mathbf{r}_r) + \theta(\mathbf{r}_f;\, \mathbf{r}_r) \tag{A4}$$

These phases are defined by the listing below:

- φ_{DI} phase of the laser illumination incident on the diffuser.
- φ_{DR} random component of phase imparted by the diffuser
- φ_0 phase contributed by any optical components and windows located in the region of interest.
- θ phase contributed by fluid with a time varying density distribution.
- φ_F phase contributed by fluid with a density distribution that does not change with time.

Substituting these phases in equation (A3), the field at the image point is given by

$$U(\mathbf{r}_f) = \int\int Ae^{j\varphi_{DI}}e^{j\varphi_{DR}}e^{j\varphi_0}e^{j\varphi_F}e^{j\theta}d\mathbf{r}_r \tag{A5}$$

The usual assumption is that A varies slowly as a function of $\mathbf{r}_r$. In fact, this assumption is invalid when observations are made within an order of magnitude of the resolution limit

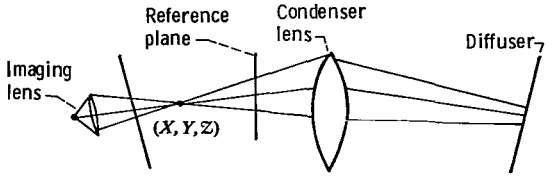

Figure 13. - Imaging of rays passing through (X,Y,Z) when illuminated by holocamera configuration of figure 2.

determined by the limiting aperture of the combined hologram recording and reconstruction systems. Then the laser speckle effect (ref. 12) leads to a rapid variation in A. However, the periods of the interference fringes important in rapid-double-exposure holography are large when compared with the resolution limit. Only the low-frequency spatial modulation of the average intensity $\langle A^2 \rangle$ is important. This long period average is approximately constant. For convenience, let $A = 1$ subject to this understanding. The field is now given by the equation

$$U(\mathbf{r}_f) = \int\int e^{j\varphi_{DI}} e^{j\varphi_{DR}} e^{j\varphi_0} e^{j\varphi_F} e^{j\theta} \, d\mathbf{r}_r \tag{A6}$$

In rapid-double-exposure holography, a second hologram is recorded after the fluid has changed slightly. In the refractionless limit, the rays are geometrically unchanged, and the field is given by

$$U'(\mathbf{r}_f) = \int\int e^{j\varphi_{DI}} e^{j\varphi_{DR}} e^{j\varphi_0} e^{j\varphi_F} e^{j\theta'} \, d\mathbf{r}_r \tag{A7}$$

where the primes denote the second exposure. Note that only θ has changed, where θ represents that part of the fluid that changes between exposures.

In the reconstructed waves from the double exposure, the intensity at the image point of $\mathbf{r}_f$ is given by

$$I(\mathbf{r}_f) = |U|^2 + |U'|^2 + U^* U' + U U'^* \tag{A8}$$

Substituting equations (A6) and (A7) into equation (A8), the intensity is given by

$$I(\mathbf{r}_f) = |U|^2 + |U'|^2 + 2\int\int\int\int \cos\Big\{\varphi_{DI}(\mathbf{r}_f; \mathbf{r}'_f) - \varphi_{DI}(\mathbf{r}_f; \mathbf{r}_r) + \varphi_{DR}(\mathbf{r}_f; \mathbf{r}'_r) - \varphi_{DR}(\mathbf{r}_f; \mathbf{r}_r)$$

$$+ \varphi_0(\mathbf{r}_f; \mathbf{r}'_r) - \varphi_0(\mathbf{r}_f; \mathbf{r}_r) + \varphi_F(\mathbf{r}_f; \mathbf{r}'_r) - \varphi_F(\mathbf{r}_f; \mathbf{r}_r) + \theta(\mathbf{r}_f; \mathbf{r}'_r) - \theta'(\mathbf{r}_f; \mathbf{r}_r)\Big\} d\mathbf{r}_r d\mathbf{r}'_r \tag{A9}$$

where $\mathbf{r}_r$ and $\mathbf{r}'_r$ are now simply dummy variables of integration. In equation (A9), only the cross-interference term has been shown explicitly. Note that the contribution of $\varphi_{DR}(\mathbf{r}_f; \mathbf{r}'_r) - \varphi_{DR}(\mathbf{r}_f; \mathbf{r}_r)$ to the argument of the cosine in equation (A9) varies rapidly with the variable $\Delta\mathbf{r}_r = \mathbf{r}'_r - \mathbf{r}_r$. Since this rapidly and randomly varying phase, which leads to the speckle effect, is of no further interest and since the details of its variation would change from one diffuser sample to another in any case, the phase factors

$$e^{\pm j[\varphi_{DR}(\mathbf{r}_f; \mathbf{r}'_r) - \varphi_{DR}(\mathbf{r}_f; \mathbf{r}_r)]}$$

are ensemble averaged. For a diffuser this average is an extremely narrow function of $\Delta\mathbf{r}_r$ and has a minimum width of the order of a wavelength of light. After a change of variables

$$\Delta\mathbf{r}_r = \mathbf{r}'_r - \mathbf{r}_r \text{ and } r_r = \mathbf{r}_r$$

the integrand is decomposed into factors that vary rapidly with $\Delta\mathbf{r}_r$ and factors that vary slowly with $\Delta\mathbf{r}_r$. The variable $\Delta\mathbf{r}_r$ is equated to zero in the slowly varying factors. These factors are then removed from the integral that depends on $\Delta\mathbf{r}_r$. It can be shown that this integral is now the same proportionality factor in all terms of equation (A9) and the integral is dropped from further discussion. Equation (A9) becomes

$$I(\mathbf{r}_f) = 2\Big\{\mathrm{p} + \int\int \cos[\theta(\mathbf{r}_f; \mathbf{r}_r) - \theta'(\mathbf{r}_f; \mathbf{r}_r)] \, d\mathbf{r}_r\Big\} \tag{A10}$$

where p is the area on the reference plane subtended by the aperture of the viewing system. Note that proportionality constants are not shown explicitly in equation (A10) or in the remainder of this paper.

The only phase that appears in equation (A10) is the change in phase associated with the time varying field as it appears at the two exposures. Define

$$\Delta\theta(\mathbf{r}_f;\ \mathbf{r}_r) = \theta(\mathbf{r}_f;\ \mathbf{r}_r) - \theta'(\mathbf{r}_f;\ \mathbf{r}_r)$$

Equation (A10) is in precisely the form required for Vest's treatment of fringe localization (ref. 8). However, the vector

$$\mathbf{r}_r \equiv (X, Y, 0)$$

refers to an arbitrary plane of reference. The salient features of the theory of fringe localization are stated as follows:

(a) An interference pattern appears to be located (localized) where its visibility is a maximum. The visibility is defined to be

$$\frac{I_{max} - I_{min}}{I_{max} + I_{min}}$$

where I_{max} and I_{min} are the maximum and minimum intensities on the surface where the pattern is measured.

(b) If a viewing direction is established by the vector $\mathbf{r}_f - \mathbf{r}_r$, then $\mathbf{r}_f$ will define a point of localization if the rays in the cone whose axis is along the viewing direction and whose apex is defined by $\mathbf{r}_f$ sum to maximize

$$\left| \iint \cos[\Delta\theta] d\mathbf{r}_r \right|$$

The base of the cone is the projection of the viewing aperture in the reference plane.

(c) The cross interference term

$$\left| \iint \cos[\Delta\theta] d\mathbf{r}_r \right|$$

will be a maximum at those points where $\Delta\theta$ is essentially a constant over the pencil of rays defined in (b); that is, $\Delta\theta$ must be stationary with respect to $\mathbf{r}_r$. It is assumed that the components of $\mathbf{r}_r$ can be varied independently: the viewing aperture should be approximately symmetrical.

From (a), (b), and (c), the localization condition is defined by

$$\nabla_r \Delta\theta = 0 \tag{A11}$$

where

$$\nabla_r \equiv \hat{\imath} \frac{\partial}{\partial x} + \hat{\jmath} \frac{\partial}{\partial y}$$

It is important to realize that equation (A11) refers to a particular viewing direction relative to the reference plane. Given a point $\mathbf{r}_r$ in the reference plane and a viewing direction defined by the unit vector

$$\mathbf{k} = \mathbf{k}_x \hat{\imath} + \mathbf{k}_y \hat{\jmath} + \mathbf{k}_z \hat{k}$$

it is true that

$$\mathbf{k} \times (\mathbf{r}_f - \mathbf{r}_r) = 0 \tag{A12}$$

By convention, the unit vector $\mathbf{k}$ will point to the center of the viewing aperture.

The set of points defined by equations (A11) and (A12) is always defined subject to the constraint that **k** is fixed. The region of interest is scanned with an imaging system whose axis maintains a fixed direction relative to the reference plane. The localization set is defined for that direction **k**. If **k** is changed, a new set of localization points will be defined that may be quite different from the previous set.

For the particular viewing direction **k**, the set of points $\mathbf{r}_f$ satisfying equations (A11) and (A12) will fall, in general, on a curved line. In some practical cases the phase change will depend only weakly or not at all on one of the two components of $\mathbf{r}_r$. Then only one component of equation (A11) will yield an equation for $\mathbf{r}_f$. Then, the localization set will fall on a surface rather than on a curved line.

Even when localization is confined to a curved line, fringes will be recognized over a nonzero volume of the region of interest. The reason is that a finite viewing aperture will have a nonzero depth-of-field for viewing fringes. Reference 8 presents a detailed discussion of this phenomenon. Briefly, in the notation of this paper and specifically for phase objects, fringe visibility away from the optimum points of localization will vary according to

$$V = \frac{\sin(\hat{\imath}\cdot \nabla_r \Delta\theta\, \delta_x)\sin(\hat{\jmath}\cdot \nabla_r \Delta\theta\, \delta_y)}{\hat{\imath}\cdot \nabla_r \Delta\theta\, \delta_x\, \hat{\jmath}\cdot \nabla_r \Delta\theta\, \delta_y} \tag{A13}$$

Here, δ_x and δ_y are half the widths of the projection of the viewing aperture cone on the reference plane. A very conservative criterion is that the fringe visibility must decline to zero before a change in fringe visibility will be detected. Using this criterion, fringe visibility will remain apparently unchanged provided that

$$\begin{aligned} -\frac{\pi}{\delta_x} &< \hat{\imath}\cdot \nabla_r \Delta\theta < \frac{\pi}{\delta_x} \\ -\frac{\pi}{\delta_y} &< \hat{\jmath}\cdot \nabla_r \Delta\theta < \frac{\pi}{\delta_y} \end{aligned} \tag{A14}$$

If desired, any criterion based on an arbitrary reduction in fringe visibility can be used to replace equation (A14). The quantitative effect of finite depth-of-field is ignored elsewhere in this paper; however, the effect is referred to qualitatively from time to time.

We may now derive the localization conditions for a time varying refractive index field. Let the change in refractive index field between the first and second exposures be denoted by $f(\mathbf{r})$. The phase change is given by the line integral

$$\Delta\theta = \frac{2\pi}{\lambda}\int f(\mathbf{r})\,ds \tag{A15}$$

Here, s is the distance along the ray defined by $(\mathbf{r}_r; \mathbf{k})$. The vector $\mathbf{r}$ is a function of the vector $\mathbf{r}_r$ and the distance s. The convention will be to measure distance from the reference plane so that

$$\begin{aligned} &\mathbf{r} = \mathbf{r}_r + s\mathbf{k} \\ &\text{and} \\ &s = z/k_z \end{aligned} \tag{A16}$$

The symbol λ represents the vacuum wavelength of the light used. Substituting equation (A15) into equation (A11), localization is given by the equation

$$\nabla_r \Delta\theta = \frac{2\pi}{\lambda}\int \nabla_r \mathbf{r}\cdot \nabla f\, ds = 0 \tag{A17}$$

From equation (A16), it follows that

$$\nabla_r \mathbf{r} = \nabla_r \mathbf{r}_r + s \nabla_r \mathbf{k} \tag{A18}$$

When equation (A18) is substituted into equation (A17), the localization criterion is given by

$$\int \nabla_r \mathbf{r}_r \cdot \nabla f \, ds + \int \nabla_r \mathbf{k} \cdot \nabla f s \, ds = 0 \tag{A19}$$

Because distance is measured from the reference plane and because $f(\mathbf{r})$ is nonzero over a finite region only, equation (A19) can be written conveniently as

$$\int_{-\infty}^{\infty} \nabla_r \mathbf{r}_r \cdot \nabla f \frac{dz}{k_z} + \int_{-\infty}^{\infty} \nabla_r \mathbf{k} \cdot \nabla f \frac{z \, dz}{k_z^2} = 0 \tag{A20}$$

Using equation (A12) and the fact that $\mathbf{k}$ is a unit vector, the six components of $\nabla_r \mathbf{k}$ can be evaluated. The components are given by

$$\nabla_r \mathbf{k} = \begin{pmatrix} -\frac{k_z}{\mathcal{Z}}(k_y^2 + k_z^2) & \frac{k_z}{\mathcal{Z}} k_x k_y & \frac{k_z}{\mathcal{Z}} k_x k_z \\ \frac{k_z}{\mathcal{Z}} k_x k_y & -\frac{k_z}{\mathcal{Z}}(k_x^2 + k_z^2) & \frac{k_z}{\mathcal{Z}} k_y k_z \\ 0 & 0 & 0 \end{pmatrix} \tag{A21}$$

For convenience, define the vectors

$$\mathbf{K}_x = [k_y^2 + k_z^2, \; -k_x k_y, \; -k_x k_z] \tag{A22}$$

$$\mathbf{K}_y = [-k_x k_y, \; k_x + k_z^2, \; -k_y k_z] \tag{A23}$$

When equation (A21) is substituted into equation (A20) and the definitions from equations (A22) and (A23) are used (eq. (1)), the condition for localization that appears in the text, is obtained, namely,

$$\mathcal{Z} = \frac{\int_{-\infty}^{\infty} \nabla f \cdot \mathbf{K}_x z dz}{\int_{-\infty}^{\infty} \hat{\imath} \cdot \nabla f \, dz} \qquad \mathcal{Z} = \frac{\int_{-\infty}^{\infty} \nabla f \cdot \mathbf{K}_y z dz}{\int_{-\infty}^{\infty} \hat{\jmath} \cdot \nabla f \, dz} \tag{1}$$

To conclude this appendix, the proper use of equations (1) is summarized.

(a) In the region where the refractionless limit applies, choose a convenient reference plane

(b) Erect a coordinate system with its x,y axes in this plane

(c) Represent the *change* in refractive index distribution between exposures by a function $f(\mathbf{r})$

(d) Evaluate the gradient of this function $\nabla f(\mathbf{r})$

(e) Recall that $\mathbf{r}$ is confined to a ray having a direction $\mathbf{k}$ and passing through the point $\mathbf{r}_f = (X, Y, \mathcal{Z})$. Hence, substitute

$$\mathbf{r} = \mathbf{r}_f + \mathbf{k}\frac{(Z - \mathcal{Z})}{k_z}$$

into the gradient.

(f) Substitute the parameterized expression for ∇f into equation (1) and integrate.

Steps (a) to (f) will yield, in general, two equations for $\mathcal{Z}$ as a function of X and Y. Be aware that one of the two equations may not exist except in a trivial sense.

Appendix B

Effect of Wavelength Changes on Fringe Localization

In rapid-double-exposure holography, a hologram is recorded with a pulsed laser and reconstructed with a continuous wave laser. In general, the wavelengths of the lasers used for recording and reconstruction will be different. In the case of a ruby, helium-neon combination

$$\mu = \frac{\lambda_{\text{He-Ne}}}{\lambda_{\text{ruby}}} = \frac{6328\ \text{Å}}{6943\ \text{Å}} = 0.911$$

and in the case of a frequency-doubled Nd:YAG, argon-ion combination

$$\mu = \frac{\lambda_{\text{ion}}}{\lambda_{\text{Nd:YAG}}} = \frac{5145\ \text{Å}}{5320\ \text{Å}} = 0.967$$

As shown in this appendix, this change in wavelength can be treated as an imaging defect, and has no other effect on fringe localization.

From equation (A4) in appendix A, the phase of each ray at the photographic plate can be expressed by

$$\varphi(X,Y,Z,x,y,0) = \sum_i \varphi_i + \theta \tag{B1}$$

where the phases φ_i are the time invariant phases found in equation (A4) and where the phase θ is the phase associated with the time varying fluid. For a second exposure the phase of the same ray is given by

$$\varphi'(X,Y,Z;x,y,0) = \sum_i \varphi_i + \theta' \tag{B2}$$

The ray in equations (B1) and (B2) intersects the photographic plate at some point. Call the phase of the reference beam at that point, φ_r and the phase of the reconstruction beam at the same point, φ_c. The analysis of Meier (ref. 13) is used in this discussion.

The phases of the reconstructed rays are given by

$$\varphi(X,Y,Z;x,y,0) + \varphi_c - \varphi_R = \sum_i \varphi_i + (\varphi_c - \varphi_R) + \theta \tag{B3}$$

$$\varphi'(X,Y,Z;x,y,0) + \varphi_c - \varphi_R = \sum_i \varphi_i + (\varphi_c - \varphi_R) + \theta' \tag{B4}$$

The phase difference $\varphi_c - \varphi_r$ along with $\sum_i \varphi_i$ is a constant between exposures and has no effect on fringe formation. However, when $\varphi_c - \varphi_r \neq 0$, the ray will be deviated at the hologram. This deviation is an imaging defect and can be grouped with similar defects in the remaining imaging system. The analysis is developed in the following paragraphs.

Recall from appendix A that localization requires that a pencil of rays passing through any point in the region of interest be collected and refracted to a point image by an imaging system. The following defects are possible in any imaging system, including a hologram where $\varphi_c - \varphi_r \neq 0$

(a) There may be a scale transformation between the object and the image

(b) The scale factors may vary as a function of direction

(c) The scale factors may vary as a function of position (distortion)

(d) A point image may not be formed even though diffraction effects are ignored.

Effects (c) and (d) are aberrations and will occur, in general, when different wavelengths are used to record and to reconstruct holograms. From Meier, phases like $\varphi + \varphi_c - \varphi_r$ can be expanded in powers of $1/S$ where S represents distance(s) from the hologram. The

contributions from terms of order $1/S$ lead to effects (a) and (b), while terms of order $1/S^3$ lead to aberrations.

The aberrations must be negligible for double-exposure holography to be useful. Hence, the hologram aberrations are neglected along with the aberrations introduced by the other optical components.

To show that the scale transformations simply scale the line or surface of fringe localization, let the scale transformation be defined by

$$\begin{aligned} x' &= ax \\ y' &= by \\ z' &= cz \end{aligned} \tag{B5}$$

Different scale factors are assumed for the different axes. Recall that the general conditions for fringe localization are given by equations (A11). For any function $F(X,Y,Z,x,y,0)$ the scale transformation is performed by replacing F with

$$F\left(\frac{X'}{a}, \frac{Y'}{b}, \frac{Z'}{c}; \frac{x'}{a}, \frac{y'}{b}, 0\right)$$

Hence, $\Delta\theta(X,Y,Z;x,y,0)$ is replaced by

$$\Delta\theta\left(\frac{X'}{a}, \frac{Y'}{b}, \frac{Z'}{c}; \frac{x'}{a}, \frac{y'}{b}, 0\right)$$

The same localization criteria apply to the scaled reconstructed image, that is,

$$\begin{aligned} &\frac{\partial}{\partial x'}\Delta\theta\left(\frac{X'}{a}, \frac{Y'}{b}, \frac{Z'}{c}, \frac{x'}{a}, \frac{y'}{b}, 0\right) \\ &\frac{\partial}{\partial y'}\Delta\theta\left(\frac{X'}{a}, \frac{Y'}{b}, \frac{Z'}{c}; \frac{x'}{a}, \frac{y'}{b}, 0\right) \end{aligned} \tag{B6}$$

From equations (B6), it is also true that

$$\frac{\partial\Delta\theta}{\partial x'/a} = 0 \qquad \frac{\partial\Delta\theta}{\partial y'/b} = 0 \tag{B7}$$

However, on substituting equations (B5) into equations (B7), equations (A11) are obtained. Hence, (X,Y,Z) is a point of localization in the unscaled image if and only if $(X',Y',Z',)$ is a point of localization in the scaled image.

Scaling deforms the fringe according to the scale factors a, b, and c. The direction cosines of a ray are also altered. For example, if

$$k_x = \frac{X-x}{\sqrt{[(X-x)^2+(Y-y)^2+Z^2]}}$$

then

$$k_x' = \frac{X-x}{\sqrt{[(X-x)^2+(b/a)^2(Y-y)^2+(c/a)^2Z^2]}}$$

so that

$$k_x \neq k_x'$$

In general, it will be possible to select a position for the reconstruction source so that the scale transformation is cancelled in one plane. Even though $a=b=1$, it will be true that $c\neq 1$. Cancellation of all three scale transformations will be impossible when $\mu\neq 1$.

Cancellation of the scale transformations can be summarized adequately in the paraxial approximation (ref. 13). For a z-axis perpendicular to the hologram, the transverse magnification (magnification perpendicular to the z-axis) is given by the equation

$$M_V=\frac{1}{\left[1+\frac{z_0}{\mu Z_c}-\frac{z_0}{z_R}\right]}$$

where the symbol M_V refers to the transverse mangification of the virtual image, where z_0 is the axial distance of an object point from the hologram, where z_R is the axial distance of the reference source from the hologram, and where z_c is the axial distance of the reconstruction source from the hologram.

Clearly, $M_V=1$ if $z_c=z_R/\mu$. On the other hand, the longitudinal magnification (magnification along the z-axis) is given by $M_L=M_V^2/\mu$. When $M_V=1$, $M_L=1/\mu$. Hence, there will be a longitudinal extension of the virtual image when $\mu\neq 1$ even when the transverse magnification is unity.

In the paraxial approximation, the angular magnification is given by $M_A=\mu$ regardless of the choices for M_V and M_L.

To summarize, points of localization are transformed by the combined recording and reconstruction processes in the same way that other object points are transformed. As with other object points, the integrity of the fringe may be destroyed by aberrations. The magnification when $\mu\neq 1$ cannot be cancelled in all directions. If measurements of fringe position are to be made relative to a particular direction, magnification can be equated to unity in that direction. For a ruby, helium-neon combination, suppose that the longitundinal magnification is equated to unity. Then the transverse magnification is given by $M_V=\mu=0.954$. Hence, for this combination the maximum error due to the change in wavelength will be less than 5 percent of the maximum dimension measured.

Appendix C

Symbols

A	magnitude of electromagnetic field
A_i	coefficients in polynominal representation of shock wave
a	number having arbitrary size in representation of shock wave
a,b,c	scale factors (appendix B)
$\mathbf{d}$	translation vector
E	localization error
$\bar{\mathbf{E}}$	unit tensor
e_0	slope of shock wave at first exposure in planes parallel to yz-plane (eq. (37))
F	function
$f(\mathbf{r})$	field of refractive index change
$g(\mathbf{r})$	function representing shock wave surface
h_0	slope of shock wave at first exposure in planes parallel to xz-plane (eq. (37))
$dh/d\alpha$, $de/d\alpha$	variation with rotor angle α of slope of shock wave at second exposure (eqs. (38) and (39))
I	intensity
i	summation index
$\hat{i},\hat{j},\hat{k}$	unit vectors defining Cartesian axes
$\mathbf{K}_x$	$[k_y^2+k_z^2, -k_xk_y, -k_xk_z]$
$\mathbf{K}_y$	$[-k_xk_y,\ k_x^2+k_z^2, -k_yk_z]$
$\mathbf{k}$	unit vector establishing viewing direction, $[k_x,k_y,k_z]$
M_A	angular magnification
M_L	longitudinal magnification
M_V	transverse magnification of virtual image
N,N_0	refractive index function for shock wave
ΔN	change in refractive index across shock wave
n	ratio of shock strengths for two exposures $n \equiv [\Delta n(\mathbf{R})/\Delta n(\mathbf{R}_t)]$, also used for refractive index (appendix A)
Δn	$1-n$
p	area of projection of viewing aperture on reference plane
$\mathbf{R}$	position in reference frame at which viewing axis crosses shock wave at first exposure
$\mathbf{R}'$	position in reference frame at which viewing axis crosses shock wave at second exposure
R_c	tip radius of compressor rotor
$\mathbf{R}_t$	position in transformed frame at which viewing axis crosses shock wave at second exposure
$\mathbf{r}$	position vector in reference frame, $\equiv(x,y,z)$
$\mathbf{r}_f$	position vector at point on interference fringe (localization point) in reference frame, $\equiv(X,Y,Z)$
$\mathbf{r}_r$	position vector of point in reference plane
$\mathbf{r}_t$	position vector in transformed system
S	used for $\hat{f}\cdot R$ in main text; designates generally curved ray in appendix A; designates distance from hologram in appendix B

s	distance along a light ray
U	denotes electromagnetic field associated with light ray at first exposure
U'	denotes electromagnetic field associated with light ray at second exposure
V	fringe visibility
$X,Y,\mathcal{Z}$	Cartesian coordinates of point on interference fringe (point of localization)
x,y,z	Cartesian coordinates in reference frame
x_t,y_t,z_t	Cartesian coordinates in transformed coordinate system
Z	axial coordinate in reference frame at which viewing axis crosses shock wave at first exposure
Z_t	axial coordinate in reference frame at which viewing axis crosses shock wave at second exposure
z_c	axial distance of reconstruction source from hologram (appendix B)
z_0	axial distance of object point from hologram (appendix B)
z_r	axial distance of reference source from hologram (appendix B)
α	angular rotation of compressor rotor between exposures
$\bar{\Gamma}$	Cartesian tensor of direction cosines
δ_x,δ_y	half widths of projection of viewing aperture on reference plane
θ	phase of time varying fluid at first exposure
θ'	phase of time varying fluid at second exposure
λ	vacuum wavelength of light
μ	ratio of wavelength during reconstruction to wavelength during recording of hologram
σ	standard deviation
φ	phase
φ_c	phase of reconstruction beam at hologram
φ_{DI}	phase of laser illumination incident on diffuser
φ_{DR}	phase imparted by diffuser
φ_F	phase contributed by time invariant fluid
φ_0	phase contributed by optical components and windows
φ_r	phase of reference beam at hologram
$\bar{\Omega}$	tensor, $-\hat{\imath}\hat{k}+\hat{k}\hat{\imath}$ (*dyadic notation*)
∇	vector differential operator $\hat{\imath}\,\partial/\partial x+\hat{\jmath}\,\partial/\partial y+\hat{k}\,\partial/\partial z$
∇_r	vector differential operator in reference plane only $\hat{\imath}\,\partial/\partial x+\hat{\jmath}\,\partial/\partial y$
∇_t	vector differential operator in transformed coordinate system $\hat{\imath}\,\partial/\partial x_t+\hat{\jmath}\,\partial/\partial y_t+\hat{k}\,\partial/\partial z_t$
$\nabla g(\mathbf{R})$	implies differentiation with respect to Cartesian coordinates followed by substitution of $\mathbf{R}$
$\nabla_t g(\mathbf{R}_t)$	implies differentiation with respect to transformed coordinates followed by substitution of $\mathbf{R}_t$

References

1. Strazisar, A. J.; and Powell, J. A.: Laser Anemometer Measurements in a Transonic Axial Flow Compressor Rotor. NASA TM-79323, 1980.
2. Wuerker, R. F.; et al.: Application of Holography to Flow Visualization Within Rotating Compressor Blade Row. (AIRESEARCH-73-9489, AiResearch Mfg. Co.; NASA Contract NAS3-15336.) NASA CR-121264, 1974.
3. Collier, Robert J.; Burckhardt, Christopher B.; and Lin, Lawrence H.: Optical Holography. Academic Press, 1971.
4. Heflinger, L. O.; Wuerker, R. F.; and Brooks, R. E.: Holographic Interferometry. J. Appl. Phys., vol. 37, no. 2, Feb. 1966, pp. 642-649.
5. Koechner, W.: Solid-State Laser Engineering. Springer-Verlag, 1976.
6. Decker, A. J.: Holography Through Optically Active Windows. NASA TP-1414, 1979.
7. Powell, J. Anthony: Electronic Angular Position Encoder Apparatus. U.S. Patent 4,171,522, Oct. 16, 1979.
8. Vest, C. M.: Holographic Interferometry. John Wiley & Sons, Inc., 1979.
9. Thomas, J. B.: An Introduction to Statistical Communication Theory. John Wiley & Sons, Inc., 1969, pp. 582-584.
10. Strazisar, A. J.; and Chima, R. V.: Comparison Between Optical Measurements and a Numerical Solution of the Flow Field in a Transonic Axial Flow Compressor Rotor. AIAA Paper 80-1078, June, 1980.
11. Howes, W. L.; and Buchele, D. R.: A Theory and Method for Applying Interferometry to the Measurement of Certain Two-Dimensional Gaseous Density Fields. NACA TN 2693, 1952.
12. Decker, A. J.: Analytical Procedure for Evaluating Speckle Effect Instrumentation. NASA TM X-3478, 1977.
13. Meier, R. W.: Magnification and Third-Order Aberrations in Holography. J. Opt. Soc. Am., vol. 55, Aug. 1965, pp. 987-992.

1. Report No.	2. Government Accession No.	3. Recipient's Catalog No.
NASA TP-1868		

4. Title and Subtitle	5. Report Date
FRINGE LOCALIZATION REQUIREMENTS FOR THREE-DIMENSIONAL FLOW VISUALIZATION OF SHOCK WAVES IN DIFFUSE-ILLUMINATION, DOUBLE-PULSE HOLOGRAPHIC INTERFEROMETRY	April 1982
	6. Performing Organization Code 505-32-82
7. Author(s)	8. Performing Organization Report No.
Arthur J. Decker	E-757
	10. Work Unit No.
9. Performing Organization Name and Address	
National Aeronautics and Space Administration Lewis Research Center Cleveland, Ohio 44135	11. Contract or Grant No.
	13. Type of Report and Period Covered
12. Sponsoring Agency Name and Address	Technical Paper
National Aeronautics and Space Administration Washington, D.C. 20546	14. Sponsoring Agency Code

15. Supplementary Notes

16. Abstract

A theory of fringe localization in rapid-double-exposure, diffuse-illumination holographic interferometry is developed. The theory is then applied to compare holographic measurements with laser anemometer measurements of shock locations in a transonic axial-flow compressor rotor. The computed fringe localization error is found to agree well with the measured localization error. It is shown how the view orientation and the curvature and positional variation of the strength of a shock wave are used to determine the localization error and to minimize it. In particular, it is suggested that the view direction not deviate from tangency at the shock surface by more than 30^{o}.

17. Key Words (Suggested by Author(s))	18. Distribution Statement
Holography; Holographic interferometry; Flow visualization; Fringe localization; Compressors; Shock waves; Pulsed laser; Transonic flow; Turbomachinery	Unlimited - Unclassified STAR Category 35

19. Security Classif. (of this report)	20. Security Classif. (of this page)	21. No. of Pages	22. Price*
Unclassified	Unclassified	42	A03

* For sale by the National Technical Information Service, Springfield, Virginia 22161

NASA-Langley, 1982

National Aeronautics and
Space Administration

Washington, D.C.
20546

Official Business
Penalty for Private Use, $300

THIRD-CLASS BULK RATE

Postage and Fees Paid
National Aeronautics and
Space Administration
NASA-451

U.S.MAIL

/ 1 1U,J, 070732 S0905.03
DEPT OF THE AIR FORCE
AF WEAPONS LABORATORY
ATTN: TECHNICAL LIBRARY (SUL)
KIRTLAND AFB NM 87117

NASA

POSTMASTER: If Undeliverable (Section 158 Postal Manual) Do Not Return